Masterarbeit

Vorklinische Verifikation eines Bestrahlungsplanungssystems mit Monte-Carlo Dosisberechnung und biologischer Optimierung

ausgefürt an der Technischen Universität Wien
und der Univ.-Klinik für Strahlentherapie
Medizinische Universität Wien/ AKH Wien

unter der Anleitung von

Univ.-Doz. Dipl.-Ing. Dr. Dietmar Georg

durch

Irina Fotina
Pfeilgasse 4-6/810
1080 Wien

Wien
20.03.2008

Master Thesis at the Vienna University of Technology
for obtaining the M.Sc degree

Pre-clinical verification of a treatment planning system with Monte-Carlo dose calculation and biological optimization

BSc Irina Fotina

Supervisor

Univ.-Doz. Dipl.-Ing. Dr. Dietmar Georg

Division of Medical Radiation Physics
Department of Radiotherapy
Medical University of Vienna
Währinger Gürtel 18-20, A-1090 Vienna

Vienna
March 20, 2008

Aknowledgments

Without the help and support of my colleagues, family and friends I would not have been able to write this work.

First of all, I want to thank Dr. Dietmar Georg for his optimism, attention and stimulating discussions. It is entirely owing to him that I was able to work with his team and receive financial support for my studies in Vienna. Also I'm thankful for his irreplaceable and careful reading and corrections.

I'm much obliged to Prof. Richard Pötter, Department of Radiotherapy, AKH Wien, for use of the equipment.

My special thanks to Dr. Bernhard Kroupa for his patience in answering all my questions. He actually opened for me the area of IMRT treatment planning and I learned a lot from his practical experience. He supported me a lot during the process of execution and writing of this work. I'm very grateful to Thomas Künzler for his support and unforgettable discussions and advices even on subjects outside of professional topics. I would like to thank Dr. Markus Stock for his great solutions of the technical problems during my measurements and Dr. Peter Winkler for helping me just simply a lot, especially with LaTeX issues. At last but not least, I want to say thanks to all colleagues, creating the great working climate and even more great coffee-breaks.

Special thanks goes my friends Ekaterina Matina, Alyona Cherepanova, Sergey Galushin, Tchigorko Anton, Alyona Terra, Leonid Potapov and Roman Ostvald for their mental support despite of the 8000 km distance between us, Nadezhda and Alexander Schukoff, Veronica Vejvodova, Aina Catala Blasco, Paula Castellano Mico and Esther Sancho Llorens for making my stay and studies in Vienna unforgettable, eventful and fruitful. For my greatest motivation and the most important feeling of understanding and support I owe the biggest thanks to my sometimes and somewhere complicated but still very important relationship, to the one person who makes me feel special.

Finally I would like to express my sincere thanks to my parents Eugeny and Tatjana Fotina, who made my studies possible, for their continuous mental and financial support, encouragement and just for their unlimited believe in me.

Thank you!

Contents

Abstract

In IMRT the combination of hardware and software techniques solves the problem of irradiating complex target volumes with concave parts in the close vicinity of critical structures, a problem with which planners had to struggle from the very beginning of radiotherapy. The approach of inverse planning for IMRT requires a special software tools for the solution of optimization problem and achievement of the required accuracy of the dose calculation.

The evolution of treatment planning systems for IMRT offers some improvements and a number of modern solutions for the dose calculation and optimization. The aim of this thesis was to investigate IMRT treatment planning with TPS Monaco™ and to perform measurements for its commissioning and subsequent verification of the IMRT treatment plans.

Monaco™ combines Monte Carlo dose calculation algorithm and biologically expressed objective functions. These two innovating features imply some specialties on commissioning measurements and planning process. Monte Carlo dose calculations aim to provide excellent level of accuracy for the dose calculation with insignificant prolongation of the planning time. Use of the biologically-based objective functions makes the planning process easy and transparent for any corrections and an EUD formalism of optimization constraints helps for the plan analysis and evaluation.

For the patient-specific plan validation we used dedicated phantoms, where IMRT plans were recalculated. The measurements with EBT films and ion chambers were performed and compared with the results from the treatment planning system. All results obtained with Monaco™ were inside the established acceptance criteria, which was also confirmed by verification on the independent software for monitor unit verification. The acceptable dose deviation for ionization chamber measurements and MU verification should be below 3% and criteria for γ-index verification also deal with 3 mm distance-to-agreement and 3% dose difference, expressed in terms of γ_{mean} and $\gamma > 1$.

The issues on planning and verification procedures together with respective results described in this thesis enable a safe implementation of such TPS into the clinical routine, but some follow-up dosimetric tests and further exploration of the system possibilities for different planning solutions are highly recommended.

Abbreviations

BEV - Beam's Eye View
CRT - Conformal Radiotherapy
CT - Computer Tomography
CT-to-ED - CT numbers to Electron Density
CTV - Clinical Target Volume
DMLC - Dynamic Multileaf Collimation
DTA - Distance-To-Agreement
DVH - Dose Volume Histogram
EPID - Electronic Portal Imaging Device
EUD - Equivalent Uniform Dose
FSPB - Finite Size Pencil Beam
FSU - Functional Sub-Unit
GTV - Gross Tumor Volume
HU - Hounsfield Unit
IAEA - International Atomic Energy Agency
ICRU - International Commission on Radiation Units and Measurements
IMAT - Intensity Modulated Arc Therapy
IMRT - Intensity Modulated Radiotherapy
ITV - Internal Target Volume
LDEM - Local Dose Effect Measure
Linac - Linear Accelerator
MC - Monte Carlo
MIMiC - Multileaf Intensity Modulating Collimator
MLC - Multileaf Collimator
MRI - Magnetic Resonance Imaging
MU - Monitor Unit(s)
NTCP - Normal Tissue Complication Probability
OAR - Organ At Risk
OD - Optical Density
PB - Pencil Beam
PDD - Percentage Depth Dose
PET - Positron Emission Tomography
PTV - Planning Target Volume
QA - Quality Assurance
RT - Radiation Therapy
ROI - Region Of Interest
RMS - Root Mean Square
SIB - Simultaneous Integrated Boost
SMLC - Segmental Multileaf Collimation

SPECT - Single Photon Emission Computer Tomography

SSD - Source-to-Surface Distance

TCP - Tumor Control Probability

TERMA - Total Energy Released per unit MAss TPS - Treatment Planning System

VEFM - Virtual Energy Fluence Model

XVMC - X-ray Voxel Monte Carlo

2D - Two-dimensional

3D - Three-dimensional

Chapter 1

Introduction to IMRT

1.1 Contemporary role of IMRT

Over the past two decades, enormous progress has been made in radiation therapy. A lot of scientific and clinical methods were developed for increasing the therapeutic efficiency of cancer treatment with radiation. The foremost goal of radiotherapy practice is to encompass all cancer cells with sufficient doses of radiation during each fraction, while simultaneously sparing surrounding normal tissues. In the early stage of radiotherapy, only square or rectangular fields were available. The methodology was significantly improved by using additional shielding blocks in a radiation fields. Thus, the beam shapes could individually be conformed to the respective projections of the target. This so-called conformal radiotherapy (CRT) was further facilitated by the advent of multileaf collimators (MLC), as time efforts and workload were drastically reduced. Three-dimensional conformal radiation therapy (3DCRT) is a technique of irradiating a target volume that is defined in three-dimensions by anatomic image of the patient with a set of x-ray beams individually shaped to conform the two-dimensional beam's eye view (BEV) projection of the target. 3DCRT became feasible with the development of computed tomography (CT).

Intensity-modulated radiotherapy (IMRT) emerged in clinical practice as a result of the development of three-dimensional conformal radiotherapy (3DCRT) in the mid-nineties. The basic idea of IMRT is to modulate the intensity across a beam. The added flexibility (compared to conventional beams of uniform intensity) can be utilized to achieve a higher degree of spatial agreement ("conformality") of the resulting high region of a dose distribution within the tumor target volume, as shown on the figure 1.1. Typically, in IMRT we reduce the intensity of rays that go through particularly sensitive critical structures and increase the intensity of those rays that see primarily the target volume. The resulting hot and cold areas are compensated by corresponding cold and hot areas from intensity-modulated beams from other directions. Thus, IMRT relies heavily on synergistic effects from multiple beams.

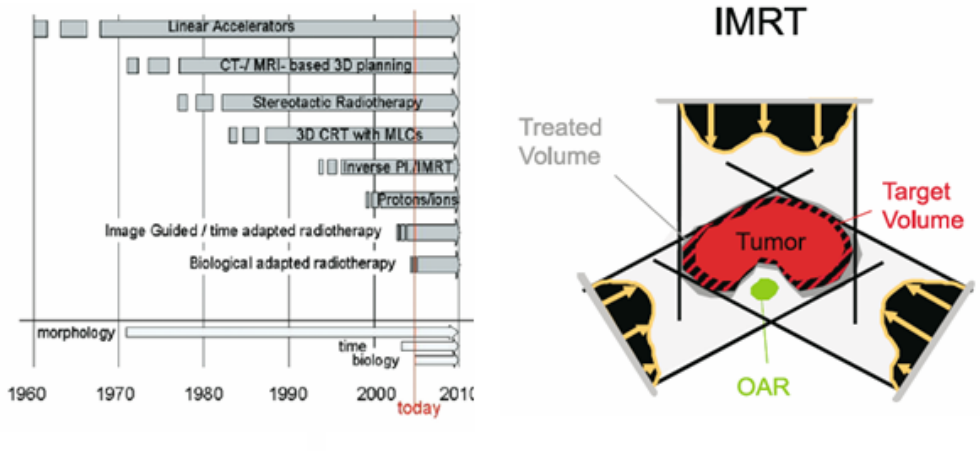

Figure 1.1: Place of IMRT in a historical development of external beam radiotherapy and illustration of the IMRT principle. (OAR - organ at risk) [9, 57].

With a reference to the recent book "Imaged-guided IMRT" (editors: T. Bortfeld, R. Schmidt-Ullrich et al) the definition of IMRT can be describes as follows: *"IMRT is a radiation treatment technique with multiple beams incident from different directions in which at least some of the beams are intensity modulated so that each beam intentionally delivers a non-uniform dose to the target. The desired dose distribution in the target is achieved after superimposing such beams. The additional degrees of freedom to adjust intensities of individual rays are utilized to achieve a better target dose conformality and/or better sparing of critical structures"* [9].

In IMRT the combination of hardware and software techniques solves the problem of irradiating complex target volumes with concave parts in the close vicinity of critical structures, a problem with which planners have had to struggle from the very beginning of radiotherapy. The most advantageous applications of IMRT are:

- treatment of concave target volumes. The most prominent example is that of the prostate planning target volume when the PTV overlaps the rectum and especially when seminal vesicles are involved;
- treatment of arbitrarily shaped targets (including convex ones), surrounded by or being in the vicinity of complex normal tissue anatomy (head-and-neck cancer);
- capacity to deliver the same or different doses per fraction to different targets simultaneously (This is so-called simultaneously integrated boost (SIB) technique). An example of the former is the simultaneous stereotactic radiotherapy of multiple brain nodules.

However, IMRT with photon beams also has a definite limitations starting from physical depth-dose characteristics of high-energy photon beams dose distributions, trade-offs during optimization process and involvement of the different uncertainties (imaging, positioning, dose

Figure 1.2: A multileaf collimator (MLC). Design of Varian Medical Systems of Palo Alto, California (left) and Elekta. Source: http://www.elekta.com; http://www.varian.com.

calculations, biological and physical changes of tumor and normal tissue etc.,). The evolution of treatment planning systems for IMRT offers some improvements and a number of modern solutions for the dose calculation and optimization will be presented in the next chapters.

1.2 IMRT delivery techniques

Different approaches for the IMRT delivery were developed during last decade and one of the possible ways to classify them is the division into fixed-gantry angle or arc-based IMRT. In general, the difference between these techniques is that three-dimensional dose distribution is achieved with a superposition of segmental fields from either a number of fixed directions or a number of directions distributed on one or several arcs. In the Department of Radiotherapy, Medical University of Vienna/General Hospital of Vienna, the fixed-gantry approach is employed since 2001. For that reason, the detailed description of arc-based techniques is behind the scope of this work.

1.2.1 Fixed-gantry techniques

Fixed-gantry techniques started their development from the use of simple blocks for intensity modulation and revealed their potential within the use of multileaf collimator (MLC)1.2. Detailed reviews of the history and performance of MLCs for 3D CRT are given by Webb [70, 71]. The use of MLCs for static or dynamic IMRT is discussed in more detail in another work by Webb (2004) [72]. Using linac-integrated MLC for the IMRT, an intensity map is decomposed into a set of MLC-formed apertures and can generally be divided into "step-and-shoot" delivery and "dynamic modes".

Step-and-shoot MLC delivery The "step-and-shoot" (also "stop-and-shoot" or segmental MLC delivery, SMLC) is a straightforward extension of a multiple field irradiation technique.

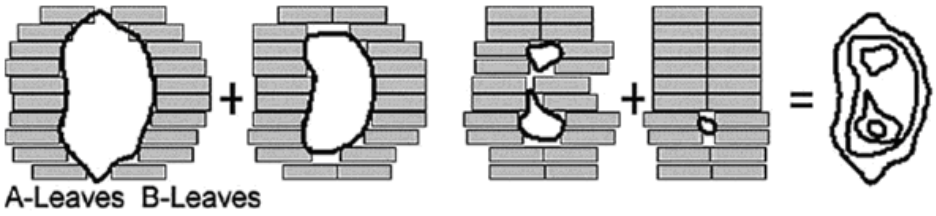

Figure 1.3: Principle of "step-and-shoot" IMRT delivery [57].

The "step-and-shoot" approach superimposes the dose delivered by a number of irregularly shaped and partially overlapping treatment fields, called segments (see Fig.1.3). For each segment a well-defined number of monitor units (MU) is delivered. Then, the beam is turned off while the leaves of the MLC move to the positions required by the next IMRT segment. This process is repeated for all segments per incident beam angle and all beam directions, respectively.

The mechanical characteristics of MLCs are very important for IMRT delivery. Spatial resolution of created fluence maps is limited by leaf width perpendicular to the direction of leaf movement; and along the direction of leaf movement by the maximum overtravel and precision of leaf positioning. The effects of the leakage and transmission also should be taken into account. The decomposition of a flunce map for a given case into deliverable segments is called sequencing. Most inverse treatment planning programs have a build-in leaf-sequencing algorithm. The total number of segments depends on the complexity of the fluence maps, number of intensity levels, the number of beams, and other technical factors. Since the total treatment time depends linearly on the number of segments, a significant effort is put into optimizing the sequencing algorithm to find the best solution in terms of treatment time. At the Medical University of Vienna IMRT treatments are currently delivered with the SMLC technique. The main reasons are: a standard MLC can be used, verification and control of treatment fields is relatively fast, interrupted treatments can be easily resumed. The detailed information about dosimetrical and mechanical evaluation of the SMLC dedicated linear accelerator (LINAC), as well as description of the commissioning test for the segmental IMRT delivery done in the department, are extensively described by Kroupa and Georg (2002-2005) [28, 37].

Dynamic MLC delivery For the "dynamic" or "sliding window" delivery technique (DMLC) the intensity modulation is achieved by an individual variation of the velocities of the moving leaves, i.e., the treatment can be realized without interrupting the treatment beam, as shown on the figure 1.4.

The clinical application of this technique was pioneered at the Memorial Sloan Kettering Center in New York in 1998 [14, 41]. The total treatment time for the "dynamic" MLC technique is mostly shorter than the one to deliver the same fluence pattern with any "step-and-shoot" approach. The main disadvantage of this approach is that dose rate and leaf velocity can not be arbitrarily chosen. In addition to the technical properties required for an MLC to be used in

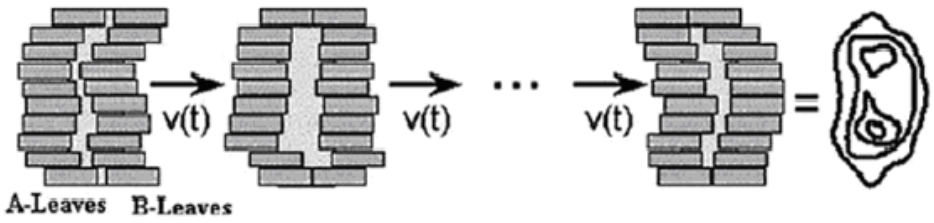

Figure 1.4: Principle of dynamic IMRT delivery [57].

static mode, the "dynamic" delivery technique requires that the leaf speed be controllable with a very high accuracy and that the calibration process for leaf speed and leaf position must be easily possible [41]. From a technical point of view the "dynamic" approach is more complex than the "step-and-shoot" approach. For the "dynamic" process the leaves are moving while the beam is turned on and therefore a very accurate control of the leaf positions, leaf speed, and dose rate at the same time must be achieved.

1.2.2 Arc-based techniques

Arc-based IMRT as treatment modality started in the early 1990s with the commercially available Peacock IMRT treatment planning system (TPS) and MIMiC fan beam delivery device (North American Scientific, NOMOS, USA) [13, 74]. Other arc-based techniques available today are two modifications of a fan beam-based approach and cone-beam technique.

Serial Tomotherapy (Original Peacock system) The basic idea beyond the fan beam techniques is that the modulation of the radiation beam can be done by a binary MLC moving in and out of a fan beam. To cover the whole target volume the radiation should be delivered slice-by-slice like in a CT scanner. The combination of the words "tomography" and "radiation therapy" lead to the expression "tomotherapy" [45], which is used nowadays worldwide. In a serial approach employed by Peacock system the table is fixed during the rotation of the gantry through 270 degrees with the radiation beam on. The fan presents as a narrow rectangular slit aperture much wider transaxially than longitudinally. After each rotation the couch is moved in longitudinal direction for the delivery of the next fan beam. The beam is collimated to a narrow slit and beamlets are turned on and off by driving the mini-MLC leaves out and in the beam path, respectively, as the gantry rotates around the patient. Each slice covers 2-4 cm thickness and up to 20 cm length. An advantage of this modality is that the MIMiC collimator can be retrofitted to an existing linear accelerator without an MLC, allowing IMRT treatment without a substantial hardware upgrade. However, reduced clearance is considered as a main disadvantage of the system.

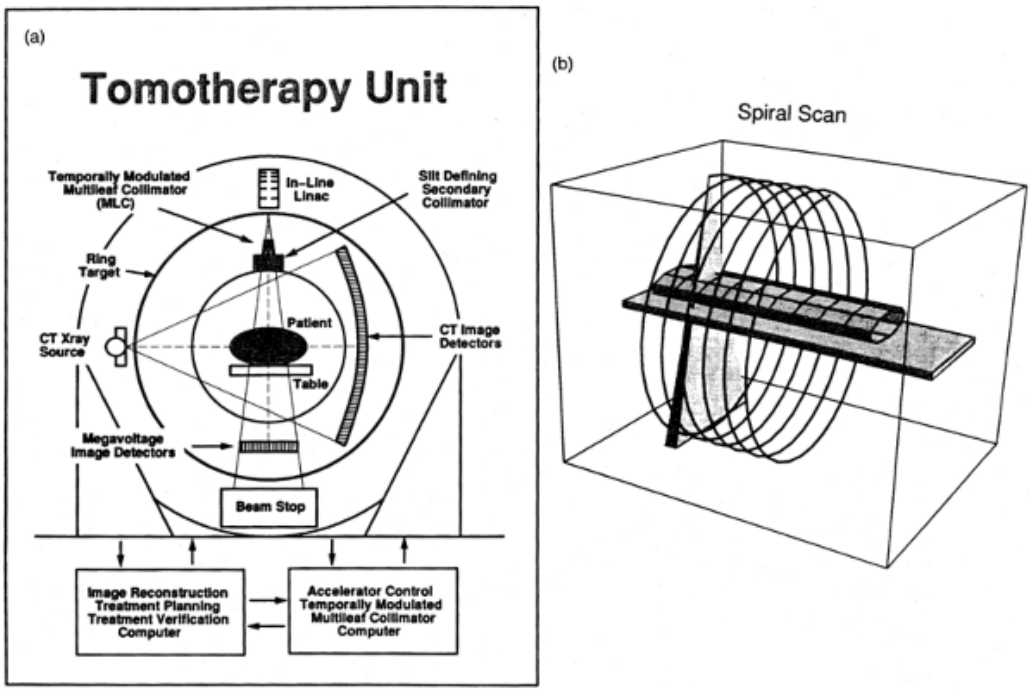

Figure 1.5: Principle of the Tomotherapy delivery [45].

Helical Tomotherapy The helical version of tomotherapy was developed by Mackie et al. [45] and is commercially available from Tomotherapy, Inc. USA. Here, a linear accelerator of 6MV is mounted on a ring gantry and moves around the rotation axis (see Fig. 1.5). A pneumatic MLC is used to modulate the radiation fluence in a method similar to the Peacock system. The binary MLC of the helical tomotherapy machine consists of 64 interdigitated leaves with 32 leaves on each side. Due to the high air pressure, the leaves can open or close the radiation field within only 40 ms. Unlike the Peacock system, the Tomotherapy system moves the patient couch at the same time the gantry is rotated, providing a delivery geometry that is helical in nature. An added feature of the Tomotherapy system is an imaging system that is placed opposite the radiation source. This allows the Tomotherapy system to be used as a megavoltage CT system for on-board patient imaging [17, 44].

Intensity modulated arc therapy (IMAT) To date, the majority of work on arc-based IMRT has been focused on modulated fan beams, and little development has been done using cone beams. Intensity-modulated arc therapy (IMAT) was invented by Yu in 1995 [79] as a logical development of the multiple static field IMRT techniques. In IMAT the gantry rotates several times, corresponding to the number of subfield components, delivering each component from each gantry angle at each rotation. These components are chosen so that leaves movement from one gantry rotation to another is minimized. When a single arc is used for treatment, the technique is sometimes called aperture-modulated arc therapy. At this time, there are no extensive information defining how many arcs are sufficient for any disease sites, but with the

commercial products devoted to IMAT (for instance from Elekta, Crawley, UK), and in some cases as few as three rotations are sufficient [80].

1.3 Treatment planning for IMRT

The first important step in IMRT treatment planning, which is the most time-consuming part in the IMRT treatment chain, is the selection of the patient. For many patients the benefits from IMRT are negligible and with conventional 3D CRT the treatment goals can be fulfilled completely. Besides the advantages for the treatment of concave targets near organs at risk and the potential for dose escalation, availability of a good positioning systems and the ability of the patient to tolerate longer time for simulation and treatment should be taken into account. At the Medical University of Vienna majority of indications for IMRT are head-and-neck and gynecological cases.

IMRT is characterized also by the integration of the different imaging modalities into the planning process. The basic information for the definition of target volumes and other structures, as well as information about electron density necessary for the dose calculation, is obtained via planning CT scan. In a case if CT images are not satisfying for the definition of planning volumes, other imaging modalities as MRI (magnetic resonance imaging), PET (positron emission tomography), SPECT (single photon emission tomography) and ultrasound, can be employed. Functional MRI and PET are also very important in context of the rapidly developing field of biological adaptive radiotherapy and the introduction of biological optimization into IMRT treatment planning.

The simulation of IMRT patients is similar to the process for patient undergoing conformal treatment, and conventional simulation or virtual simulation can be used. TPS Monaco™ (Computerized Medical Systems, CMS, USA) has the module for virtual simulation process, with principles and interface identical to the FocalSim™ (CMS). This software module is also used as a basic tool for the volume definition and creation of DRRs.

For the search and computation of the optimal beam intensities corresponding to the desired fluence distribution IMRT relies on inverse treatment planning, because the number of beamlets to be optimized, makes the optimization very complicated. At present there are many computerized optimization codes developed for the IMRT treatment planning. They include 3D imaging modalities for the definition of target volumes and critical structures, different dose calculation algorithms and optimization solutions. The detailed description of these features from TPS Monaco™will be provided in the dedicated chapters. In the following only some remarks together with the general information about treatment planning workload for IMRT (see Fig.1.6), applicable to any modern TPS, will be discussed.

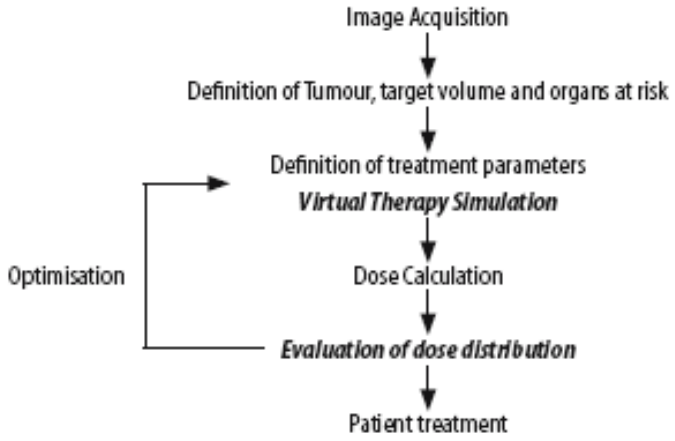

Figure 1.6: Radiotherapy planning cycle [57].

1.3.1 Structure delineation

Since the dose calculation, optimization and plan evaluation are based on the 3D patient model, the definition of anatomic structures and delineation of target volumes is one of the crucial steps in the planning process. According to guidelines established by the International Commission on Radiation Units and Measurements (ICRU) [6, 7], the gross tumor volume (GTV) and the clinical target volume (CTV) should be contoured (see Fig.1.7). Radiation oncologists are in charge of defining these volumes, but the other structures, like planning target volume, can be created by medical physicists. So the next step would be the definition of planning target volume (PTV) in order to take into account set-up uncertainties, machine tolerances and intra- and intertreatment variations. The definition of the PTV is as follows: " *The planning target volume (PTV) is a geometrical concept, and it is defined to select appropriate beam arrangements, taking into consideration the net effect of all possible geometrical variations, in order to ensure that the prescribed dose is actually absorbed in the CTV (ICRU Report No. 50)*".

The PTV concept has a special importance not only for the dose prescription but also for dose reporting and, thus, the evaluation of plans. The main criteria applied to PTV are, that the PTV coverage with the 95% of the prescribed dose should exceed 95% of the volume and the maximum dose value for IMRT plan should not exceed 115% of the prescribed dose. For IMRT planning, the dose prescription guidelines often need to be complemented by additional parameters to obtain acceptable dose distributions. Usually they are used in a form of dose-volume combinations, but prescriptions based of equivalent uniform dose (EUD), tumor control probability (TCP), or normal tissue complication probability (NTCP) can be also employed.

In Monaco™ different tools for the delineation of the volumes of interest are available, starting from simple 2D manual drawing to 3D reconstruction of margins. The names of the structures

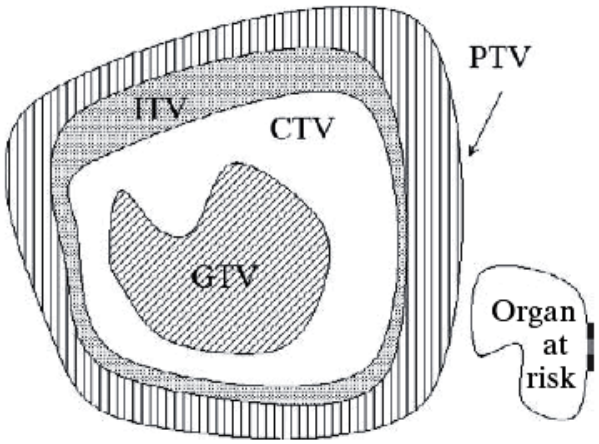

Figure 1.7: Graphical representation of the volumes of interest, as defined in ICRU Reports 50 and 62 [54].

can be chosen freely, except for the external contour of the patient, that should be the same on the QA dedicated study set. Also the consequent choice of the beam energy and gantry angles is done at the same sofware module as the one used for delineation.

1.3.2 Inverse treatment planning

As indicated previously, IMRT requires a computer optimization method of determining the nonuniform beam-fluence profiles that lead as close as possible to the desired dose distribution. Roughly speaking, inverse problems can be described as problems in which the output or consequences are known but not the cause. The difference between inverse planning modules of various treatment planning systems lies in the specifications of the input and output parameters and the criteria used to select the final solution. Specific to RT, the output is generally specified by a desired dose distribution, a set of desired dose-volume histograms (DVHs), or even the TCP or NTCP for the involved structures. Typically, the number of beams and their incident directions are determined empirically before dose optimization [49].

In 1982, Brahme et al. [12] developed the concept of determining the modulated radiation field fluence distribution necessary to produce a desired dose distribution. In 1989 Cormack and Quinto proved that for general mathematic solutions, the optimized fluence profiles can contained unphysically realizable solution, that is to say, negative intensity [15]. In subsequent years different numerical solutions were developed in order to determine physically deliverable incident fluence maps. With a reference to [39] reported methods and models for fluence optimization include:

- exhaustive search (Barth,1990);

- gradient techniques (Xing and Chen 1996; Spirou and Chui 1998; Bortfeld 1999; Seco et al. 2002; Zhang et al. 2004);
- image reconstruction approaches (Brahme et al. 1988; Bortfeld et al. 1990; Holmes et al. 1991);
- simulated annealing (Webb 1989; Mohan et al. 1992; Djajaputra et al. 2003);
- superposition algorithm (Scholz et al. 2003) and several others techniques.

in general, the task of generating an optimal treatment plan can be separated into two parts:

1. specification of an optimization criterion;
2. the optimization algorithm used.

Objective function The optimization criterion is expressed as a mathematical entity in the form of **an objective or cost function**. The objective function defines a plan's quality and is to be maximized or minimized, as appropriate, to satisfy a set of mathematical constraints. Historically, most objective functions use dose-based or dose-volume-based criteria, but recent efforts are examining the use of biologically based indices (e.g., tumor control probability and normal tissue complication probability [51, 78], which are a subject of a special interest for this work.

In planning systems the results of the optimization process are presented in a form of dose points, isodose curves and surfaces, dose-volume histograms, maximum, minimum and average dose values, EUD values and optionally as TCP and NTCP curves for a given structure. Dose-volume histograms summarize the information about 3D dose distribution and can be displayed as cumulative or differential DVH. DVH plots the volume (sum of the voxels inside the region of interest) as a function of dose and represents the powerful tool for the plan analysis and evaluation (see Fig: 1.8). In Monaco™ at present only differential DVH representation is available together with the dose statistics, where maximum, minimum and average dose values together with 2 flexible user-defined dose-volume points are displayed.

1.3.3 Treatment plan validation

Some processes for QA of IMRT treatment plans are the same as for conventional plans. Examples are patient-specific QA procedures for the verification of the patient positioning, obtaining portal films or images for the comparison with DRRs, verification of the machine output and dosimetrical measurements. Electronic portal imaging (EPID) gives a possibility to check separately intensity modulated beams [68] and can be used instead of surface dosimetry, which is not suitable for the IMRT verification, because of the high fluence gradients, large amount of different segments for the beam delivery and multiple angles of incidence. One of

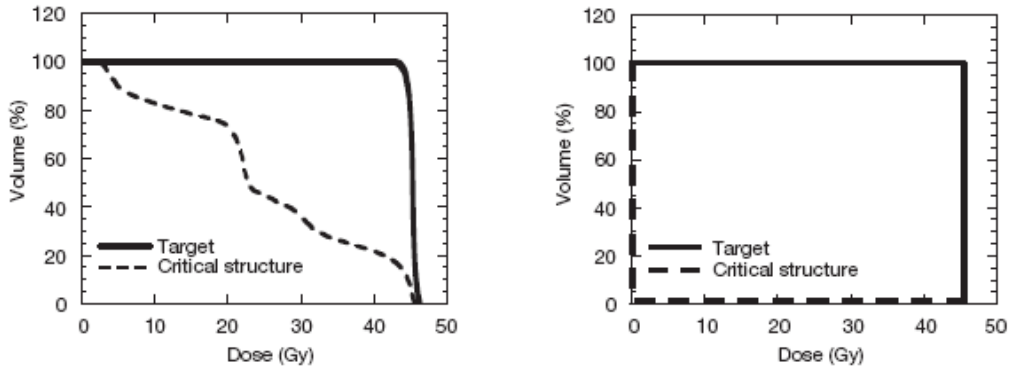

Figure 1.8: Example of a cumulative DVH for a case target-OAR together with the ideal DVH [54].

the widely used techniques of the patient-specific plan validation is the use of the dedicated phantoms, where IMRT plans are recalculated and then the measurements with films and ion chambers are performed. These measurements are compared with the results from the treatment planning system and compared with the results of the treatment planning system. Typically, ion chamber measurements should agree within $\pm 3\%$, whereas film is often evaluated as a percent discrepancy or distance to agreement (typically 3% or 3 mm) [65]. Initially, this type of analysis should be performed for all IMRT patients. Some centers have eliminated film dosimetry after verifying several hundred patient plans [36].

In IMRT the treatment-planning system provides the MUs for each field. The MUs are verified either by direct measurement [42] or by an independent calculation system [29]. Manual or simple software calculation has been found useful to double check the monitor unit of a treatment plan. Such software uses the fluence maps and MUs generated by the treatment planning system to independently calculate the dose to the isocenter.

1.4 Objectives of this thesis

Intensity modulated radiotherapy is used today in increasing number of centers worldwide. The fast development of the different software programs for the IMRT treatment planning holds the promise for improving radiotherapy. The IMRT planning system Monaco™ (CMS) is promoted as one of the most advanced solutions on the market, because of the implementation of biologically assisted cost functions in the optimization process and also it features a Monte Carlo dose calculation algorithm. The aim of this thesis is to provide the description of the process of pre-clinical verification of a treatment planning system for IMRT. The information about preparatory steps as basic beam data acquisition, some commissioning tests, treatment planning process and verification of IMRT plans will be discussed. In addition information about available dose calculation algorithms and optimization solution represented in Monaco™ will be given in a separate chapter. Later a planning solutions for typical IMRT cases, such

as head-and-neck cancer treatment with a simultaneously integrated boost technique and gynecological case, are discussed and compared with the treatment planning system Oncentra MasterPlan 3.0 (Nucletron, NL), employed in a clinical routine. Concerning the IMRT verification, three techniques were applied: film dosimetry, ionization chamber measurements and independent software for the MU verification. The final results and analysis of the data are presented in the dedicated chapter.

Chapter 2

System software and dose calculation algorithms

2.1 Dose calculation algorithms

Dose calculation algorithms are the most critical software component in a treatment planning system. The accuracy requirements for the advanced radiation therapy telling us leave a quite narrow window for the tolerable uncertainty of the dose calculation. Brahme [11] concluded that the relative standard deviation of the mean dose in the target volume should be less than 3% to achieve an absolute standard deviation of less than 10% in tumor control probability. Taking into account all patient-related geometrical uncertainties, position and motion errors, intraobserver variability in target volume delineation, mechanical factors and dosimetric uncertainties, a more realistic limit for the standard deviation between the prescribed dose and the dose delivered to the target volume is ±5% (one standard deviation). Hence the goal for the dose calculation accuracy of a TPS is 3%. The dose calculation modules in planning systems are responsible for the correct representation of dose distribution in the patient within these limits and are calculating the MU or beam time of an accelerator. There are different types of a dose calculation algorithms implemented in today‘s planning systems, which are described in the following.

The correct prediction of the dose inside the volume of interest is an important part of the IMRT optimization process. Dose values are used to evaluate the cost functions during optimization process, determine the intensities of an individual beamlet for the plan and, finally, judge and evaluate the plan. Another important aspect for the dose calculation is not only the question: “How precise is the dose calculation?”, but also “How fast is the dose calculation process?” During IMRT optimization the large solution space of beamlet intensities is explored and number of iterations can rise up to thousands in a case of complex cost functions with multiple parameters. In all calculation algorithms there is a trade-off between the final accuracy of the

dose calculation and dose calculation speed.

Dose calculation algorithms can be generally divided into correction-based or model-based algorithms. Correction-based algorithms were developed for the "homogeneous" patient, consisted from water [21]. They rely on a set of measurements of tissue-air ratios, tissue-phantom ratios, output factors etc. measured in a water phantom or in air under reference conditions. The dose in a patient is then calculated by extrapolation of these results under certain correction factors to a certain treatment fields.

Broad beam algorithms Broad beam algorithms are correction-based dose calculation algorithms [46] and they are usually not applicable for IMRT dose calculation. They are designed for the use with radiation beams that have nominally uniform fluence distribution (open or blocked field). These algorithms use measured dose distribution in a homogeneous water phantom as a function of a field size, depth, off-axis distance, and surface to source distance, etc. However, sometimes broad beam algorithm are used occasionally for aperture based IMRT optimization [20] and can also be utilized as a secondary monitor unit checking programs for IMRT QA [22, 23].

Models based on the first principles of energy transport in a matter give necessary description of the energy deposition inside the patient.These model-based algorithms give more realistic description of the absorbed dose, because patient anatomy is transfered from Hounsfield units to electron density information in a calculation grid. According to this density information the dose kernels, which describe the energy transport and deposition, are scaled to consider inhomogeneities. These model-based algorithms are the standard dose calculation algorithms in commercially available treatment planning systems.

Pencil beam algorithms The simplest form of a model-based algorithm, the so-called pencil-beam (PB) algorithm, is still the fastest dose engine [8, 47, 48]. It utilized measured data together with pencil beam energy deposition kernels derived from measurements or Monte Carlo calculations. PB algorithms don't account internal heterogeneities and surface irregularities. The PB algorithms have significant speed advantage, and are the most commonly used method for dose calculation in IMRT optimization. However because of the limitations for the dose calculation accuracy they are often accompanied by other algorithms in order to improve the final dose calculation accuracy.

Superposition or convolution algorithms Superposition or convolution algorithms [2, 59] are more accurate and sophisticated, because they separate the energy coming from the primary photon fluence and secondary radiation generated within the patient. The total energy released per unit mass (TERMA) released by the primary photon fluence is calculated and than superimposed over or convolved with the secondary energy spread kernels giving the final dose distribution [1, 10, 47]. They take into account the tissue heterogeneities for the TERMA

calculation and are much more accurate than PB in a case of complex geometries. Still the dose calculation speed is relatively long in order to be used for the whole IMRT optimization process [62, 75, 77], but it is recommended to use them after the end of the optimization for final dose calculation.

Monte Carlo approach Monte Carlo dose calculation includes all features of the energy-tissue interaction and compute directly the dose in the patient. In Monte Carlo methods individual particles are simulated first in a linac phase space, based on the design of a treatment head for a particular accelerator, including MLC. The second step is a simulation of the particle tracks and calculation of the energy deposition inside the patient. Monte Carlo algorithms are considered as the most accurate dose calculation algorithms since they directly account for tissue heterogeneities and make no assumptions regarding radiation equilibrium. The critical point in application of Monte Carlo for IMRT optimization is calculation time and influence of the inherent statistical inaccuracy, but the development of the fast algorithms such as XVMC [24, 25], VMC++ [35], and DPM [60] together with the noise reduction techniques reduce the calculation time to routinely acceptable limits.

Dose calculation algorithms implemented in Monaco™ are the so-called finite size pencil beam algorithm together with Monte Carlo calculation dose engine. These algorithms will be described in more detail in the following.

2.1.1 The FSPB algorithm

The finite size pencil beam is a primary dose calculation algorithm implemented in Monaco™ for the fluence optimization (first stage) and can be used optionally for the final dose calculation procedure. It was utilized in order to provide the necessary speed of the IMRT optimization. The FSPB algorithm is a quite simple model-based algorithm, working with the pencil beam kernel - an extension of the point-spread kernel.

The point-spread kernel $F(\vec{r}, \vec{r}', E)$ indicates the distribution of absorbed energy in water at the coordinate $\vec{r}$,which is created by interactions of primary photons of energy E at the coordinate $\vec{r}'$. A pencil-beam kernel is obtained through the integration of all point-spread kernels along an infinite ray of photons in the medium as indicated in Fig.2.1.

It is evident that the pencil beam kernel uses the more condensed information about the dose in water along the central kernel axis, i.e., it provides a coarser sampling of the physical processes than the point-spread kernel and it is therefore harder to adapt the dose calculations based on pencil beam kernels to regions with tissue inhomogeneities. On the other hand, pencil beam kernels bear the obvious advantage of reduced dose calculation times [57].

The concept of finite size pencil-beam kernel assumes that the radiation beam can be geometrically divided into identical finite size pencil beams that allow to reconstruct the dose distribution of the full beam by superposition. These finite size pencil beams are self-consistent

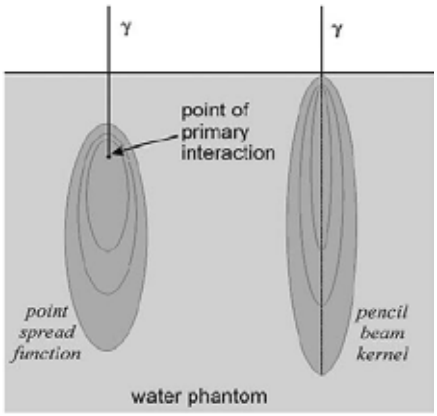

Figure 2.1: Point kernels and pencil-beam kernels [57].

in the sense that they can be used to construct arbitrary field shapes, or conversely, do not depend on the broad beam from which they were derived. The parameters for the finite size pencil-beam kernel are derived from the Monte Carlo simulations.

The detailed description of the FSPB algorithm can be found in papers of Jelen and Alber [32, 33]. In fact, it represents an analytical function with parameters determined by a fitting procedure from cross-profiles of the broad beam dose distributions calculated with Monte Carlo. This function describes the shape of the kernel and includes depth dependence derived also from the Monte Carlo simulations of dose-depth curves. The main features of this algorithm are following:

- It was especially designed for the purpose of beamlet-based IMRT optimization.
- It is sufficiently fast (4000 beamlets per min on 3 mm^3 calculation grid size on the Intel DualCore processor, 2,66GHz).
- Penumbra modeling assure physically feasible gradients in dose distribution.
- Lateral density correction is applied.
- MLC leaf shape effects like tongue-and-groove and inter-leaf scatter are excluded.

2.1.2 Monte Carlo dose calculation

In order to calculate the dose distributed in the patient the so-called transport equation must be solved. The transport equation is different for each patient and it also depends on treatment conditions such as beam directions, field sizes, energy, etc. It can be solved numerically using MC methods by simulating a large number of so-called particle histories. In this context a particle history is given by the path of one photon or one electron entering the calculation geometry until the whole energy is absorbed or until the particle and all secondary particles

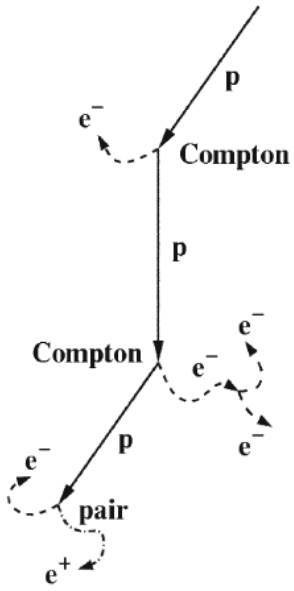

Figure 2.2: Example of a photon history in the Monte Carlo simulation of radiation transport. [57].

have left the volume of interest (see Fig.2.2). On this path, energy and momentum of the particles can change and secondary particles can arise because of interaction processes with tissue molecules. The features of these processes are determined by probability distributions given by the total and differential interaction cross sections. Sampling process parameters in a random fashion from these probability distributions forms the basis of MC simulations in radiation physics.

The input to Monte Carlo dose calculations is the fluence exiting from the treatment head, i.e. all relevant parameters depending from the accelerator. This *fluence engine* can be obtained via MC simulation or multisource model and then used for the calculation of the second part, i.e., energy transport in a patient - *dose engine*.

Beam modeling The dose calculation accuracy is strongly influenced by the quality of the treatment head model. Ideally this model should be realised by a Monte Carlo simulation of the whole linac head geometry (see Fig.2.3) using a program code system such as BEAM [56]. For that purpose a geometric model of all linac head components (target, primary collimator,flattening filter, secondary collimators, etc.) must be created. Then photon and electron transport can be simulated through the whole geometry taking into account the correct material compositions. Unfortunately, this is still time-consuming.

A possible solution of the calculation time problem is the use of phase space files. In these files parameters are stored such as position, direction, energy or charge of all particles hitting a plane below the collimating system. This plane is called phase space plane (see Fig. 2.3). During

the beam commissioning process a phase space file containing a huge number of particles is produced. Later on this plane (and file) can be used as source for the Monte Carlo transport simulation through the patient. A serious problem in this approach is the lack of information about the properties of the electrons hitting the target. Furthermore, it is impossible or at least difficult to measure these parameters. Therefore, a fitting procedure is required to adjust the electron source parameters using measured dose distributions in water and/or air. A whole treatment head simulation including a dose calculation in water and/or air with high statistical accuracy must be started each time a source parameter has changed; thus, a large number of simulations is necessary, i.e. models of this kind are inconvenient for the clinical practice.

A more practical option is to determine the features of the photon sources in the target and the photon and electron sources below the target (filter) using measurements [27]. Photons mainly have their origin in the target (primary photons) or in the flattening filter (secondary or scatter photons). The main source for electron contamination is also the filter. The features of the electron contamination source as well as the photon energy spectrum can be determined using measured depth dose distributions in water. However, this type of model makes sense only for the upper part of the linac head, i.e. for the part independent on the patient geometry and the treatment plan. Especially the beam collimating devices, such as the multi-leaf collimator, should be integrated directly into the Monte Carlo simulation [26]; thus, it is possible to model effects such as inter-leaf leakage, inter-leaf transmission, tongue-and-groove effects or the influence of rounded leaf ends.

This second approach for the beam modeling is called Virtual Energy Fluence Model (VEFM) and was developed by Fippel [27]. It is implemented in the X-Ray Voxel Monte Carlo code (XVMC) [24], designed especially for the treatment planning purposes on the base of VMC code, used for dosimetric purposes in medical physics.

Within the framework of this thesis beam data were acquired for the VEFM accelerator head models of 2 linacs (Elekta Synergy Platform with MLCi and Elekta Synergy with Beam Modulator (Elekta,Crawley,UK)) at the Department of Radiotherapy, Medical University of Vienna. The percentage depth dose and profiles in air are necessary for the head modeling and corresponding measurements in water phantom serve for the verification purposes. All particles, coming from the accelerator head can be divided into three groups:

- Primary photons, originating from the collisions of electrons with the target P_0
- Photons, scattered on the primary collimator and flattening filter P_S
- Electron contamination due to scattering processes P_e

The VEF model is composed of 2 Gaussian photon sources and an uniform electron source, representing the part of the linac head, without taking into account secondary collimator and MLC. Here the source representing the electron contamination is very small in comparison with the two photon sources, so relative electron and photon contributions satisfy following

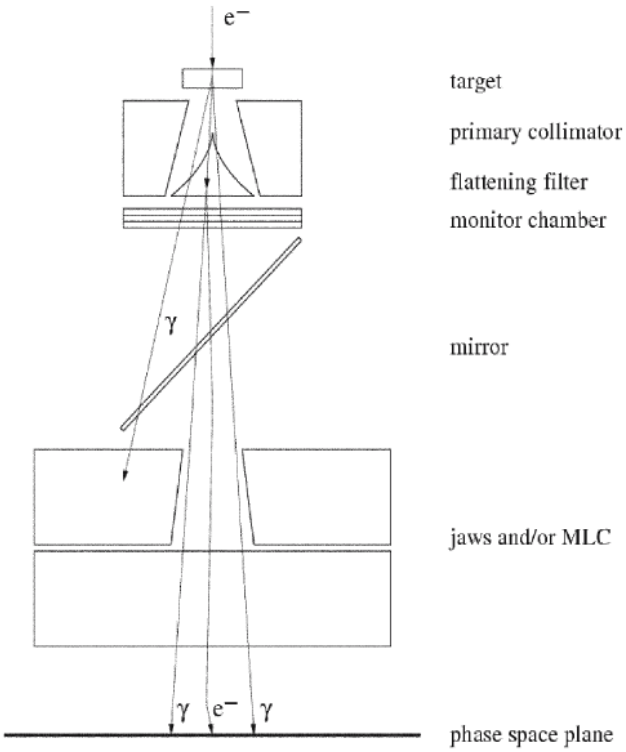

Figure 2.3: A Monte Carlo Model of the linac head geometry. [57].

equations:

$$P_e + P_\gamma = 1 \tag{2.1}$$

$$P_\gamma = P_0 + P_S = 1 \tag{2.2}$$

As shown on the Fig.2.4 the primary photon source will be represented by plane z_0 and scattered photons with the electron contamination source are on the plane z_S, corresponding to the position of the flattening filter. The distance $z_0 - z_S$ as well as the position of the other planes (jaws, MLC) are derived from the geometrical parameters of the accelerator. The standard deviations from the Gaussian sources σ_0 and σ_S are determined with the least-square fit of in-air measurements. The nominal field size is defined in X(in-plane) and Y(cross-plane) directions for the MLC and denoted as $w^M_{X,Y}$. During Monte Carlo simulations starting position of a primary photons and their direction will be determined from the planes z_X or z_Y in in-plane or cross-plane direction respectively.

The three-dimensional fluence distribution can be obtained through integration of the Gaussian function and the photon fluence is expressed as:

$$F_\gamma(x, y, z) = P_0 F_0(x, y, z) F_{cde}(x, y, z) + P_S F_S(x, y, z) \tag{2.3}$$

where term $F_{cde}(x, y, z)$ represents the central depression effect of a primary photon distribution due to flattening filter.

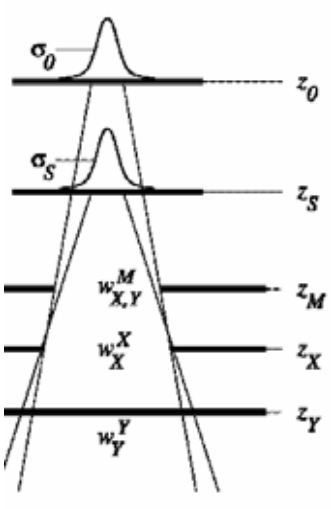

Figure 2.4: Virtual energy fluence model.

With a generation of random numbers one defines the starting position of a primary photon, with energy E (from the spectrum) and the incidence angle θ together with its probability p. All these parameters are included in the proportionality expression between energy fluence and dose in air.

$$D_{air}(x, y, z, E_\theta)dE_\theta \propto F_0(x, y, z)F_{cde}(x, y, z)E_\theta p(E_\theta, \theta) \tag{2.4}$$

Adding correction factors for build-up caps, electron contamination, and off-axis softening into parameters for Monte Carlo simulation allow to construct the full VEF model for a given linac.

XVMC Given a photon at a definite location with given momentum and energy, the first step is to sample the free path lengths until the next interaction site. By the simulation of the photon transport in a patient body the probability of path length z between two interactions is given through exponential attenuation law:

$$P(z) = 1 - exp^{-\mu(\rho,E)z} \tag{2.5}$$

with μ being the total attenuation coefficient, and ρ - the density of the medium. The photon path lengths can be sampled from this distribution using a uniformly distributed random number η_1 from interval [0,1] and the relation:

$$z = -\frac{1}{\mu}\ln\eta_1 \tag{2.6}$$

Using this path length expression the photon can be tracked to the interaction site taking into account different materials with different attenuation coefficients μ in each voxel of the calculation grid. In the energy range of radiation therapy (6 - 18 MV) μ is calculated as a sum of three relevant contributions:

$$\mu = \mu_{photo} + \mu_{Compton} + \mu_{pair} \tag{2.7}$$

with μ_{photo}, $\mu_{Compton}$ and μ_{pair} being the linear interaction coefficients or total cross sections for photoelectric absorption, Compton scattering and pair production, respectively. These parameters are different for photons of different energy. They also depend on the atomic composition of the material, i.e. they change from voxel to voxel. The interaction coefficients must be calculated from the Hounsfield units of the CT image set.

A second random number η_2 from interval [0,μ] can be used to sample the interaction type. A photoelectric absorption is simulated if η_2 is less than μ_{photo}; a Compton interaction if η_2 is larger than μ_{photo} but less than the sum of μ_{photo} plus $\mu_{Compton}$; otherwise, a pair production process is simulated.

The parameters of secondary particles after the chosen interaction, such as energy and direction, can be sampled using further random numbers and the corresponding differential cross sections for that interaction type. The formulas of the probability distributions are more complex compared with the formulas above but the sampling principle remains the same. Secondary particles are simulated like the primary particle, i.e. their transport starts with sampling the free path length to the next interaction site. The procedure continues as in the case of primary particles.

In each voxel the absorbed energy must be determined and accumulated. Later on, this leads to the dose distribution. The particle history ends if the photon leaves the calculation matrix or if its energy drops below a minimum energy (cut-off energy). The cut-off energy values implemented at the moment in Monaco™ XVMC module are 500 keV for electrons and 50keV for photons.

An extensive description of the mathematical formalism of VEFM and XVMC is behind the purpose of this thesis, but following sources [24, 26, 27] are recommended for the deep understanding of the codes.

Another important parameter is the efficiency of the Monte Carlo simulation is defined as

$$\epsilon = \frac{1}{s^2 T} \tag{2.8}$$

where s is an estimate of the variance and T is the CPU time required to obtain this variance. The statistical variance or noise in each voxel is determined by the number of simulated particle histories. The more histories are simulated, the smaller is the statistical variance. The number of histories must be increased by a factor of four to reduce the statistical variance by a factor of two, i.e. the calculation time increases by a factor of four. For an accurate dose distribution the statistical variance should be smaller than 2% relative to the maximum dose of the distribution. This accuracy can be achieved by simulating a corresponding number of histories; however, this may lead to long calculation times. Often, this time is not available in clinical practice. Therefore, other techniques and tricks are required to reduce the variance. Variance reduction techniques such as particle splitting, history repetition and Russian roulette do not require additional computer time and are widely used in Monte Carlo simulations.

Two very commonly used variance reduction techniques to improve the efficiency of the treatment head simulation are particle splitting and Russian roulette. Splitting of bremsstrahlung interactions makes optimal use of each electron track, because to follow the path of secondary photons is faster, whereas it takes a long time to track an electron in the target. Russian roulette can be played whenever a particle resulting from a class of events of little interest. The low-interest particles are eliminated with a given probability, but the weight of surviving particles is increased by the inverse of that probability.

An efficient linac and treatment head simulation algorithm plays an important role in the process of beam commissioning, but the routine utilization of the Monte Carlo code in a clinic will very strongly depend on the efficiency of the simulation in the patient. The variance reduction techniques in XVMC are history repetition, pre-calculated interaction densities and photon splitting. In history repetition one simulates an electron track in an infinite homogeneous media (typically water) and then applies the track to the actual patient geometry starting from different positions and interaction sites. With use of pre-calculated interaction densities for all voxels, one can start simulation, instead of tracing the photons incident on the patient, with the appropriate number of electrons from the different voxels.

The most significant gain in the efficiency for photon transport in the patient is obtained by combination of particle splitting and Russian roulette [35]. In this technique, N_s photon interaction sites are sampled for each incident photon using a single path through geometry. Secondary photons, resulting from Compton scattering, bremsstrahlung and annihilation, are subjected to Russian Roulette with a survival probability $1/N_s$. Surviving secondary photons are transported the same way as primary photons, and for typical patient anatomy the optimum splitting number N_s is around 40.

The Monte Carlo simulation time also depends on parameters such as energy, field size and voxel size. In case of photon beams the calculation time only slightly depends on the nominal energy. If we increase the field size, more particle histories must be simulated, i.e. the calculation time is approximately proportional to the field area. Also the voxel size is a sensitive parameter to control the calculation speed. With larger voxels the simulation can be accelerated considerably. On the other hand, spatial resolution is lost. For our calculations of IMRT plans with Monaco™ the practical value of the grid size not affecting a lot calculation time and preserving the accuracy of a dose calculation at the moment is 3 mm.

2.1.3 Sequencing

Depending on the individual case and on the specific multileaf collimator used, the translation from intensity maps to deliverable MLC patterns can introduce considerable deviations between the planned and the delivered dose. This can be attributed to the discretization of intensity levels, head scatter and leaf transmission or leakage, to the tongue-and-groove effect and to dosimetric problems with small off-axis segments or segments with very low monitor units. That's why one of the possible solutions is that these sequencing issues as well as any constraints

given by the MLC (interdigitation etc.) should be integrated into the optimization loop. This approach is called direct aperture optimization [9] and simultaneous optimization of segment weights and shapes provides the additional advantage of complete freedom in the choice of the objective function, i.e., biological objectives can be integrated easily.

It is a pattern used in Monaco™, where sequencing and MLC constraints are implemented into the second stage of the optimization process, that gives a certain flexibility while the optimization of treatment planning objectives goes together with sequencing process. It allows to create the segments adopted to the treatment goals in the second stage of the process, together with the Monte Carlo dose calculation. The "driving force" in the second stage of the optimization is an error function between the dose distribution achieved during the fluence optimization (first step) and segmented dose distribution.

The sequencer in Monaco™ requires such user-defined parameters as

- Minimum MU per segment,
- Minimum segment area,
- Segment suppression factor (minimization of flux difference between segments: $MinFlux = Min_{Area} * Min_{MU} * SegmSupF$)

The sequencing procedure in the second stage runs in three steps: smoothing, sequencing, optimization of segment weights and shapes together with plan re-optimization.

Smoothing The smoothness of fluence profiles is not a genuine condition, especially for IMRT cases, but it is of practical relevance to the reliability of treatment delivery and the simplicity of verification procedures. The idea of smoothing is not influenced by MLC constraints, but a smoother profile can be more easily translated for the sequencing procedure [3]. Smoothing can be achieved by applying of the additional term to the cost function, without effecting constraints.

$$F \rightarrow F + \lambda C^2 \tag{2.9}$$

The aim of this term is to minimize the surface on the cross-section of a beam (2.5). It can be represented as that fluence profile considered as a membrane with a surface tension and additional coefficient λ in a term for surface minimality condition C, works on increase of this tension.

Sequencing: clustering and segmentation The sequencing process of converting the optimized profile into segments has to balance two important aspects of the treatment. On one hand, the sequencing should translate the original profile as closely as possible to avoid serious deterioration of the treatment plan. On the other hand, the number of segments should be as small as possible because segment number strongly influences the treatment time. The

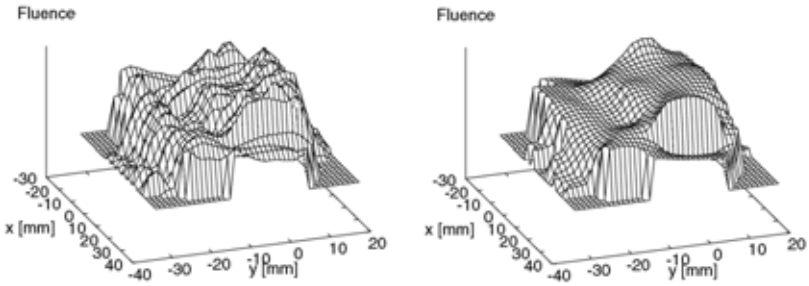

Figure 2.5: Example of a fluence profile before and after application of smoothing constraint. [3].

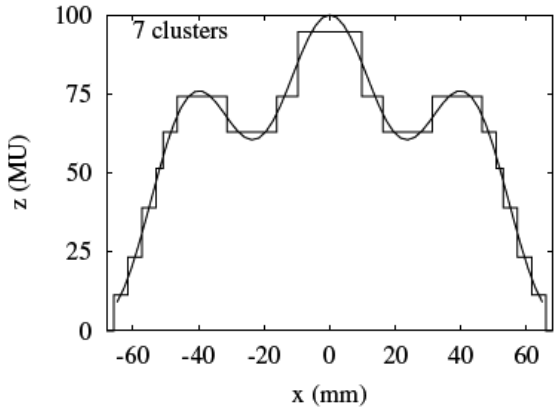

Figure 2.6: Example of a clustered profile. [5].

sequencing as part of optimization process should be fast and allow to produce slightly different but not completely new different segments after small differences in the optimized profiles.

In the clustering stage [5], the profile is projected onto a constant fluence weight (MU) profile with few levels of intensity. A constant bandwidth b, which is actually the minimal amount of MU per segment, is chosen which specifies the maximum MU deviation of any element between the value before and after the clustering. Then elements are formed to group clusters, the cluster value as one fluence weight level in the clustered profile is calculated as the mean value of all elements that belong to this cluster. An element is added to a cluster if all elements of the resulting cluster are no more than some value apart from the new cluster value.

The clustered profile has to be transformed into a series of segments before the actual treatment. The segmentation has to consider all restrictions such as the minimum field size constraint and the technical limitations of the MLC. The segmentation starts with as many segments as there are clusters (see Fig.2.6). The first segment consists of all non-zero elements, the second of all non-zero elements but those with the larger amount of MU. This scheme is repeated, so that the last segment is composed of all elements with a largest MU value. On this stage also the MLC restrictions are applied by splitting segments, or by merging them into one (if the resulting segments have the same MU and don't violate any constraints).

Segment weight optimization This part of the sequencing procedure starts with the comparison of the fluence map from the previous stage and fluence from segmented beams. The error function between two dose distributions will cause the deformation of segments and their refinement according to the optimization goals. The optimization of segment weights [4] employs a combination of a penalty function and an annealing-type escape mechanism from local minima, which can be caused by MLC constraints. After re-optimization the segments will be created again, merged or split, and dose distribution will be calculated again. The second stage finishes when there is no violation of segment-imposed constraints, and the error function reaches the certain value, but this result can lead to 3-5% dose difference in target coverage between first and second stage optimization results. This effect can be corrected by changes in objectives for targets. Second stage optimization doesn't affect the results for OARs, because in Monaco™ they are treated as hard constraints, which have to be fullfilled.

2.2 IMRT optimization

The task of IMRT optimization a complex problem with factors coming not only from a mathematical formalism but also from clinical considerations. Ideally, the goal of the optimization effort should be uniquely defined and be quite clear before the development of respective optimization strategies. Unfortunately, the definition of clinical goal is by no means clear for the detailed level of dose painting achievable with IMRT. Subtle decisions on clinical compromises between tumor doses and doses in several partially irradiated organs at risk require additional knowledge about the importance of dose homogeneity in the target, dose volume effects in organs at risk, radio-sensitivity of patient specific tissues and many more so called biological parameters. One of the advantages of "physical optimization" concepts is that they are based on quality indicators derived from verifiable physical quantities, such as dose levels and irradiated volumes, while the "biological approach" assumes additional knowledge, mostly in terms of phenomenological parameters, to characterize an observed clinical effect.

The concept of "physical optimization" was the first strategy implemented in commercial inverse planning systems and even the modifications of the original concept often referred to as "biological optimization", described below, basically keep the same logical structure of the optimization while only the mathematical formulation of the objectives of the optimization is modified. One common factor of both approaches is the selection of the energy fluence profiles for a pre-selected set of beam ports as the only treatment parameters to be optimized in the planning process.

The starting point of the optimization is a selected set of variable treatment parameters x, whose values have to be adjusted to their optimal setting x_{opt} corresponding to the desired dose distribution D_0. First, the 3D-dose distribution D is calculated for the starting, non-optimal values of x. Next, this complete 3D-dose pattern is reduced to a single number via the objective function $F(x)$. The value of $F(x)$ represents the quality of the current plan and therefore allows a ranking of different plans, i.e., the optimization of the treatment plan

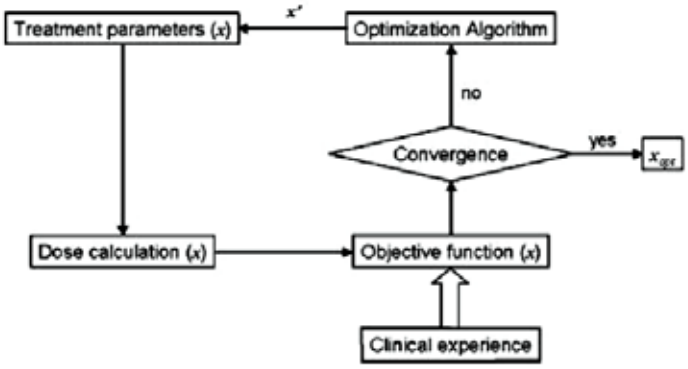

Figure 2.7: Scheme of the optimization loop. [9].

corresponds, in mathematical terms, to a search for the minimal (in most cases preferred) or maximal value of F. This is achieved with the help of the optimization algorithm, which calculates an up-dated set of x-values, labeled as $\acute{x}$ in Fig.2.7, for the next iteration of the optimization process. Often, the convergence of this "optimization loop" is stopped when a certain threshold value for the relative change of $F(x)$ between two subsequent iterations is not exceeded (or minimal difference between D and D_0 is achieved). The parameter set x found at that time is considered the result of the optimization process and will be used for the final assessment of the plan quality. This leads to the following formalism in a case of an quadratic objective function:

$$F = \frac{1}{N} \sum_n r_\sigma \left[D_c(n) - D_0(n) \right]^2 \tag{2.10}$$

where r_σ is the importance factor that weights the importance of the structure σ and parameterizes our clinical trade-off strategy and D_0 and D_c are prescribed and calculated doses, respectively. Depending on the exact expression of the objective function later we speak about physical or biologically constrained optimization.

2.2.1 Physical optimization

Dose and/or dose-volume based optimization is concerned with accurate dose distributions or DVHs of the involved structures. The quadratic objective function given in equation 2.10 represents an example of this type. Frequently, DVHs and other physical constraints (minimum or maximum dose) are imposed to describe certain clinical requirements. Dose or dose volume prescriptions are used implicitly as surrogates of the desired clinical outcome. At this point, the dose-based approach is the most widely employed method, as is evidenced by the fact that almost all commercial IMRT planning systems have chosen dose-based ranking as the starting point.

Optimization is regulated by assigning a numerical value (penalty) to a specific violation of a given constraint. The most prominent quality indicators of objective functions, the measure of

squared deviations from a given dose constraints, introduces new parameters into the optimization problem, which are not based on clinical experience but which instead are required for the mathematical formulation of the optimization problem (not convex objective functions). These quality indicators refer to one individual constraint and tissue, e.g., the standard measure is the sum of the quadratic dose deviations found for all voxels of the considered organ.

In mathematical terms for these indicators, the related function $F_T^{(-)}$ for the avoidance of an under-dosage of the target takes the form

$$F_T^{(-)}(x) = \frac{1}{N_T} \sum_{i=1}^{N_T} \left[C_+ \left(D_{min}^T - D_i^T(x) \right) \right]^2 \tag{2.11}$$

The analogue term for the avoidance of global overdosage effects for either target or OARs reads

$$F_k^{(+)}(x) = \frac{1}{N_k} \sum_{i=1}^{N_k} \left[C_+ \left(D_{min}^k - D_i^k(x) \right) \right]^2 \tag{2.12}$$

The operator $C_+(x)$ defined by $C_+(x) = x$ for $x \geq 0$ and $C_+(x) = 0$ for $x < 0$ ensures that only constraint violations contribute to the quality indicators F^+ and F^-.

Naturally, the given indicators for target structures $F_T^{(-)}$ and organs at risk $F_k^{(+)}$ refer to mutually conflicting goals of the optimization, i.e., the combination of these individual constraints is crucial for the clinical compromise achievable with that particular optimization scheme. Furthermore, and maybe even more important, the design of the overall objective function has to introduce "steering parameters" such that the planner can efficiently derive the clinically acceptable plan of his choice. Simplicity of the objective function, combined with the request that the overall objective function remains convex, leads to the well known weighted sum of individual quality indicators, i.e.,

$$F(x) = w_T^{(+)} F_T^{(+)}(x) + w_T^{(-)} F_T^{(-)}(x) + \sum_k w_k F_k^{(+)}(x) \tag{2.13}$$

With the introduced weighting factors w for each constraint the planner can now steer the result of the optimization towards the optimal treatment plan of his preference. Unfortunately the parameters w do not have any intuitive meaning and it is unknown how sensitive the outcome of an optimization is coupled to variations of the respective weighting factors. That's why optimization process based on pure dosimetric parameters is highly dependent from the experience of the physicist and suffer from lack of transparency.

Any further description of the dose-volume cost functions will be not provided in this thesis, but can be found in [39, 57]. The optimization process in Monaco™ is lead by biologically formulated cost functions. Still some of the physical objective functions are necessary (see table 2.1), and their role will be explained in the next section.

Cost function	Type	Applied to		Class
Poisson Cell Kill	Objective	Target		Biological
Parallel Complication Model	Constraint or secondary objective		OAR	Biological
Serial Complication Model	Constraint or secondary objective		OAR	Biological
Quadratic Overdose	Constraint	Target	OAR	Physical
Quadratic Underdose	Constraint	Target		Physical
Maximum Dose	Constraint	Target	OAR	Physical
Overdose Volume	Constraint or secondary objective		OAR	Physical
Underdose Volume	Constraint	Target		Physical

Table 2.1: List of the cost functions implemented in TPS Monaco™

2.2.2 Biological optimization

The dosimetric factors such as volumetric dose distribution are relatively easier to define, measure and control, as opposed to more complex biological factors. For these reasons, they have been commonly used to prescribe, record, verify, and optimize radiation treatments. However, it is the biological mechanisms that are ultimately responsible for expressing radiation-induced damage to a tumor and normal cells.

Generally, the response of the tumor and normal tissues is a function of radiation dose and volume subjected to each level of dose. Thus, at the next level of refinement, the optimization criteria could be expressed in terms of dose-volume combinations, e.g., the limit on the volume of an organ that may be allowed to receive a certain dose or higher. This has been typically the highest level of sophistication that is used in conventional planning of radiation treatments. Often this is not sufficient.

Let us consider the illustration in Fig.2.8 of a normal structure for which a constraint has been specified that no more than 25% of the volume is to receive 50 Gy. All three DVHs shown meet this criterion. However, the DVH represented by the solid curve clearly causes the least damage. One can argue that we can overcome this limitation by specifying the entire DVH. However, it can be sometimes limiting. Multiple DVHs, in fact, an infinite number of them, could lead to an equivalent damage to a particular organ, but each DVH may produce different effects on other organs and the tumor.

These considerations have led to an interest in developing quantitative models that attempt to predict the likely biological response of organs and tissues to any arbitrary pattern of irradiation. The example of these models are TCP (tumor control probability) and NTCP (normal tissue complication probability) models. The next step forward may be to supplement dose and dose-volume criteria with biological (or dose-response based) criteria. A suitable way to cast the objective function in terms of clinical and biological criteria is to employ together with TCP and NTCP indices the concept of equivalent uniform dose (EUD).

The cost functions implemented in Monaco™ are mostly expressed in a modified EUD formal-

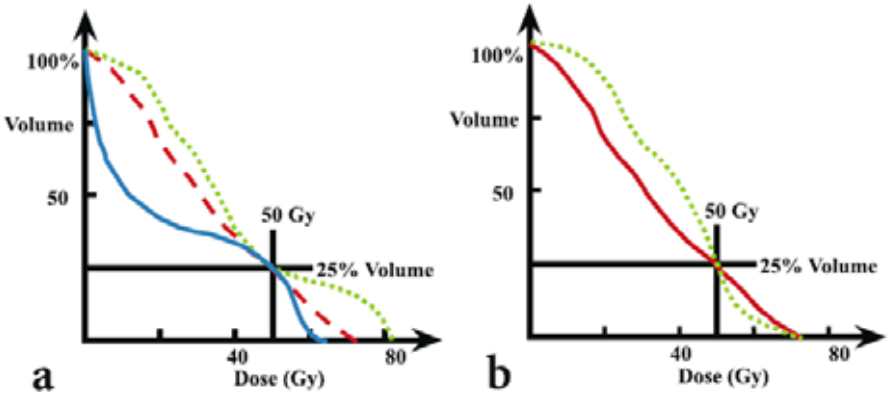

Figure 2.8: (a) Schematic representation of a normal structure DVH for which a constraint has been specified that no more than 25% of the volume is to receive 50 Gy. All three DVHs meet the criterion. The DVH represented by the solid line clearly causes the least damage. (b) Multiple DVHs can lead to an equivalent damage to a particular organ, but each DVH may produce different effects on other organs and the tumor. [9].

ism, which is called Local Dose Effect Measure formalism (LDEM) and adopted to the concept of biological optimization with mechanistic models of "critical element" or "critical volume". In the LDEM formalism all cost functions can be expressed as

$$F = \frac{1}{N}\sum_{i=1}^{N} f(D_i) \tag{2.14}$$

where D is a dose in a volume element i, N - is the number of volume elements and $f(D)$ is an objective density of a cost function (representing the weighting of a given objective function). This formalism states that the total effect for given organ or tumor is a mean of local effects and local effect function depends on a local dose in a volume element i.

The objective density can be expressed mathematically on the base of phenomenological (EUD, TCP, NTCP) or mechanistic models.

Mechanistic models Speaking about mechanistic models, we refer to Critical Element (Serial) Complication Model and Critical Volume (Parallel) Complicated Model. Here arises the fact that cells are organized structurally or functionally into Functional Sub-Units FSUs (term of Withers [73]) which in turn are organized into organs and tissues. Models which are based on the critical element assumption, and which further assume that the response of one element is not correlated with that of any other, lead to a linear complication probability vs volume relationship for small (with respect to unity) complication probabilities. The integral response model can support almost any complication probability vs volume relationship. It certainly does not have to be linear and, in the models intended application in which an organ is considered to retain function until some critical proportion of its functional units are inactivated, the integral response model has a non-linear complication probability vs volume relationship and, in particular, can exhibit a threshold effect (see Fig.2.9).

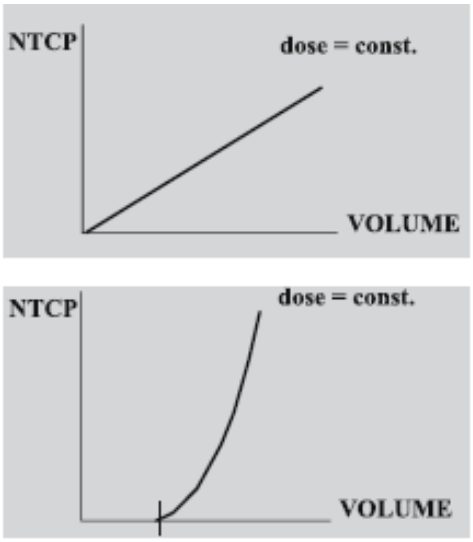

Figure 2.9: Schematic illustration of tissue architecture for the Critical Element (above) and Critical Volume (below) models [9].

Based on this definition we can divide organs-at-risk in two groups according to the volume effect.

- Serial (Critical element) organs: spinal cord, nerves, peritoneum. The structure is composed of many FSUs and irreparable damage to any one will cause a complication
- Parallel (Critical volume) organs: kidney, liver, lungs. Damage to a substantial fraction of the FSUs is necessary to cause a complication.

The main disadvantage of this approach is that in reality all organs are "mixture" of Critical elements/volumes.

Phenomenological approach In a case of phenomenological approach we have to consider the models based on clinical experience, like LKB (Lyman, Kutcher, Burman) [38, 43] and concept of EUD. In LKB model the classical NTCP notation is used:

$$NTCP(D) = \frac{1}{\sqrt{2\pi}} \int_{-\infty}^{t} e^{[-x^2/2]dx} \tag{2.15}$$

where t is defined as a function of the dose necessary to produce a 50% complication probability (TD_{50}) when uniformly delivered to the organ volume v:

$$t = \frac{D - TD_{50(v)}}{m * TD_{50(v)}} \tag{2.16}$$

where m represents slope of the sigmoidal dose-response curve.

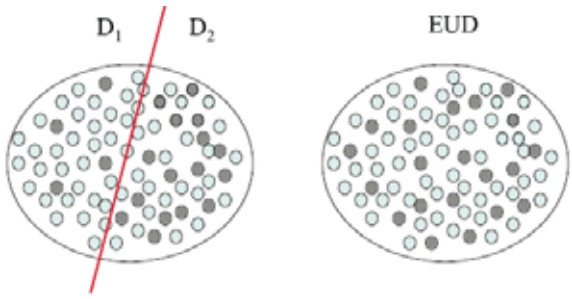

Figure 2.10: The cell survival-based EUD concept assumes that the dose distributions are biologically equivalent if the number of killed cells (illustrated as dark dots) are identical [9].

The most important aspect of the model is the assumption of the power law dependence from the partial volume v to scale TD_{50} for partial organ irradiation.

$$TD_{50(v)} = TD_{50} * v^{-n} \tag{2.17}$$

The power law exponent n describes the volume effect and the degree to which an organ exhibits serial (n decreases) or parallel (n increases) behavior. This model can be applied to different complications with only four parameters (volume of the organ, TD_{50}, n and m, obtained from fits of clinical data). These parameters are usually based on tolerance data assuming a uniform dose to an organ [19].

In reduction scheme of Kutcher and Burman not the whole organ volume is considered, but a fractional effective volume v_{ref} irradiated to a prescribed reference dose D_{ref} or the entire organ of a volume v irradiated to an effective dose D_{eff}.

$$D_{eff} = \left[\sum_i v_i (D_i)^{1/n}\right]^n \tag{2.18}$$

$$v_{eff} = \sum_i v_i (D_i/D_{ref})^{1/n} \tag{2.19}$$

According to [51], EUD represents the dose that is equivalent (in terms of the same level of the probability of local control or complication) to a given non-uniform dose distribution (see Fig.2.10). In general representation

$$EUD = \left(\sum_i v_i d_i^k\right)^{1/k} \tag{2.20}$$

and connecting $k = 1/n$, one can obtain the relationship of EUD with LKB model.

Last described shortly here, but important for further understanding of biological cost functions model is the TCP model. In a conservative representation (repopulation not included) from Poisson statistics and the LQ formalism the definition of TCP is

$$TCP = exp(-\int_v \sigma(x) exp(-\alpha(x) d(x)) dx^3 \tag{2.21}$$

where σ denotes cell density in a volume and α - cell sensitivity from linear-quadratic model.

2.2.3 Biological cost functions in Monaco™

The key concept of "iso-effects" was introduced for expressing the prescribed dose or corrections of optimization parameter. It relates the effect of the current dose distribution to standard conditions (EUD to the reference volume or fraction of volume damaged f_{dam}). The desired i.e. prescribed iso-effect is called an iso-constraint in prescription formalism of Monaco™.

Poisson Cell Kill Model In LDEM formalism the objective density of this cost function is expressed as

$$f(D(x)) = \rho(x)exp(-\alpha(x)D(x)) \tag{2.22}$$

where ρ denotes cell density and has a hard-coded value of 10^6 cells per voxel, α is the cell sensitivity, and a default value of 0.25 is recommended by software developers. This can be changed if exact knowledge about cell distribution and properties in a tumor (via fMRI/PET) are available. The user must specify the iso-constraint which is the prescribed dose in terms of EUD. The iso-constraint will be compared with the iso-effect:

$$D_{eff} = -\frac{1}{\acute{\alpha}} \log(1/V \int_V f(D(x))dx^3) \tag{2.23}$$

which is a homogeneous dose to the total volume that yields the same value of surviving cells for an average sensitivity $\acute{\alpha}$. The intrinsic exponential nature of that function tends to deliver as much dose as possible to the target. Hence, it should be limited with additional maximum dose or quadratic overdose constraints. It is necessary to mention that from various biological cost functions only the Poisson Cell Kill function is treated by the optimizer as an objective and not as a constraint. Thus the optimization process can be stopped even without the optimum results for target dose.

Serial Complication Model This model is recommended for serial organs such as the spinal cord, brainstem, rectum,nerves etc. The objective density of this function is:

$$f(D(x)) = \left(\frac{D(x)}{d_0}\right)^k \tag{2.24}$$

where d_0 is some reference dose and k is a volume effect parameter, which determines the steepness of the dose-response curve. The iso-constraint is an EUD which corresponds to maximum dose for large k (16-20) or mean dose, if k equals 1. The iso-effect is computed from

$$D_{eff} = d_0(1/V \int_V f(D(x))dx^3)^{1/k} \tag{2.25}$$

The Fig.2.11 demonstrates how the k value influence the steepness of the dose-response curve and the penalty values applied to DVHs for the serial organs.

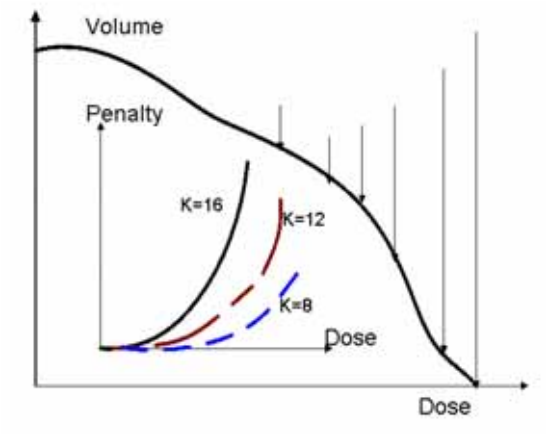

Figure 2.11: Control of the DVH curve by the Serial Complication Model cost function.

Parallel Complication Model This is a recommended constraint for the parallel organs, for example lungs or parotid glands. The objective density is given as sigmoidal function representing the probability of failure for an FSU:

$$f(D(x)) = \left(1 + \left(\frac{d_0}{D(x)}\right)^k\right)^{-1} \tag{2.26}$$

In Monaco™ the user can input parameters such as

- Reference dose which is TD_{50}
- Power law exponent k between 0.1 and 4
- Mean organ damage f_{dam}

The iso-effect is the mean damage in %.

$$v_{eff} = \frac{1}{V}\int_V f(D(x))dx^3 \tag{2.27}$$

The Fig.2.12 demonstrates how the k value influence the steepness of the dose-response curve and the penalty values applied to DVHs for the parallel organs.

The detailed examples on the prescription templates for the different IMRT study cases will be provided in the next chapter.

2.2.4 Optimization algorithms

To calculate the beam weights for a given set of constraints and a selected objective function, an optimization algorithm is required. The aim of the algorithm is to find a global minimum of the cost function. All optimization algorithms can be used for all objective functions due to the mathematical properties of the objective functions.

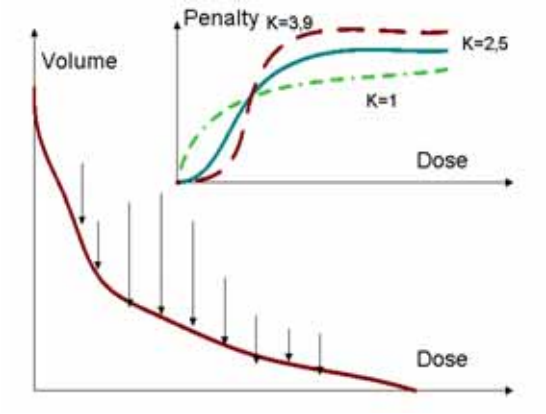

Figure 2.12: Control of the DVH curve by the Parallel Complication Model cost function.

In general, these algorithms can be divided into two categories. First, there are the deterministic algorithms like the gradient approach. These techniques are applied to optimization problems where the objective functions are convex and therefore only a global minimum and no local minima exist. For these convex objective functions like the standard quadratic objective function, deterministic algorithms can calculate the optimal solution very fast and are therefore currently used in most commercially available IMRT treatment planning systems. Second, there are the stochastic methods, like simulated annealing or genetic algorithms. They have the advantage that even for non-convex objective functions based on biological objectives or DVH-constraints the global minimum can be found even if local minima exist.

In the TPS Monaco™ two optimization algorithms are used for the different stages of IMRT optimizations. Firstly, dose-related constraints or objectives are optimized with the conjugate gradient algorithm. In the second stage of constrained aperture based optimization the simulated annealing algorithm is used, since the optimization of the segment shapes is a mathematically difficult, non-convex problem.

Conjugate gradient algorithm This algorithm takes into account the second order derivatives of the objective function for the determination of the so-called damping factor α, which controls the speed and success of the optimization. Employing a Taylor expansion of $F(x(i))$ up to the second order derivatives, one can show that a new damping factor for each iteration step is a promising alternative choice for α. For the multi-dimensional optimization problem encountered in radiation therapy (several hundred fluence amplitudes have to be simultaneously optimized) the damping factor can be expressed in terms of the inverse Hessian H^{-1} of the second derivatives of $F(x)$ [55], i.e.,

$$x(i+1) = x(i) - H^{-1}(x(i))\nabla F((x(i)) = x(i) - \alpha \nabla F((x(i)) \tag{2.28}$$

This approach calculates the Hessian at each step of the iteration and it can be shown that this version of the "conjugated gradient" approach finds the global minimum after N iterations,

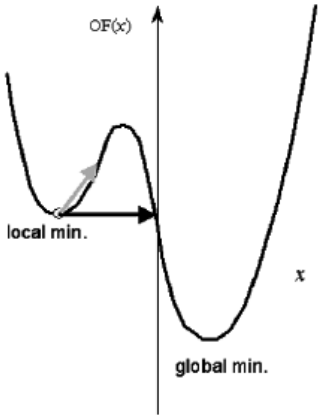

Figure 2.13: Principle of the local minima escape in simulated annealing algorithm [9].

where N is the number of optimization parameters x [55]. However, since the Hessian cannot always be calculated in a reasonable amount of time, an alternative approach is used more often for applications in radiation therapy [81].

Starting from an arbitrary point $x(0)$ the objective function is evaluated, at different positions along the line through the starting point $x(0)$ in the direction of the encountered "steepest descent", $h(0) = -\nabla F(x(0))$. This is repeated until the position of the minimum of $F(x)$ along that line is found. At the position of the minimum x_{min} the gradient $g(1) = -\nabla F(x)$ is calculated and used for the determination of the next direction in which the global minimum will be approached. The new direction for this "line minimization" approach is given by various iterative rules [55]. One potential concern with deterministic algorithms is that the iterative process may get trapped in a local minimum such that the desired global minimum is never discovered.

Simulated annealing There are basically two strategies as to how the method of "simulated annealing" escapes from the trap of local minima, "climbing uphill" and "tunneling" (see Fig.2.13). Mathematically, both described strategies involve the sampling of distributions. First, the step size $\Delta x(i)$ after i iterations ($i \geq 1$) is randomly chosen from a displacement distribution $D(\Delta x(i))$. The width of this distribution is dynamically decreasing so that smaller steps are preferred when one approaches the optimal solution. The sampling of $D(\Delta x(i))$ allows the inclusion of the "tunneling" strategy. Next, the decision whether that iteration step was a good move toward the optimal solution has to be made. This is done by random sampling of a probability distribution $P(i)$. If the difference of the objective function $\Delta F(i) = F(x(i) + \Delta x(i)) - F(x(i))$ is negative, then the new set of treatment parameters is accepted. However, in contrast to the gradient methods, the new position is also accepted with a probability $P(i)$ if the difference is positive. The probability distribution $P(i)$ for all

displacement distributions is given as

$$P(i) = \exp(\frac{-\Delta F(i)}{k_B T(i)}) \tag{2.29}$$

With the temperature $T(i)$ the width of $P(i)$ is dynamically adjusted to smaller values during the optimization process. How this "cooling" of the "up-hill" climbing is done best, depends also on the complexity of the objective function. Different combinations of $P(i)$ and $D(\Delta x(i))$ define various types of simulated annealing algorithms. For the classic simulated annealing process the starting temperature $T(0)$ is very large which leads to a higher probability to accept uphill steps. During the iteration process, the temperature is reduced and $T(i)$ must satisfy the condition $T(i) \geq T(0)\frac{1}{\log i}$ [71].

Chapter 3

Commissioning and verification of the TPS Monaco™

3.1 Data acquisition and entry

3.1.1 Beam data acquisition

Treatment planning systems require a variety of a machine and beam data, in order to provide accurate and adequate modeling of the the treatment unit with its different beam energies. Monte Carlo TPSs require accurate information concerning the geometry and composition of linac beam line components, such as the waveguide exit window, target, flattening filter, scattering foils, transmission ionization chamber, jaws, MLC, blocks and trays, and any other items the electron or photon beam is likely to encounter. This information is usually provided by linac manufacturer. A clinic has to specify the information about gantry, table and collimator rotations convention used in a particular institution.

Typical photon beam data sets acquired from a treatment unit include central axis percentage depth dose (PDD) and profiles for open and wedged fields, for a range of square fields. Sometimes diagonal profiles to account for transverse and radial beam asymmetry may also be required. Relative or absolute field size factors are required both for treatment time calculations and in the calculation of dose distributions involving dynamic beams (e.g. dynamic wedges, dynamic MLCs). Particular care must be taken with respect to the reference field size, reference depth and nominal SSD (source to surface distance), as these will have a global effect on time and MU calculations. Measured beam data relevant to the MLC can include transmission through the leaf, inter-leaf transmission between adjacent leaves and intra-leaf transmission occurring when oposed leaves meet end on.

For the treatment planning based on Monte Carlo algorithm (as well as for any algorithm

Figure 3.1: Blue Phantom

applied in today's TPS) the quality of the measured data MUST be as high as possible. Otherwise, systematic errors introduced in dose calculation. For adequate Monte Carlo simulations quite a large set of data, including in-air and water measurements needs to be obtained.

All commissioning measurements were done for two treatment units, capable to deliver IMRT: Elekta Synergy Platform with MLCi (40 pairs of leaves,1 cm width) and Elekta Synergy "S" with Beam Modulator (40 pairs of leaves, 0.4 mm width)(Elekta,Crawley,UK).

For PDD and profiles scans in water and air a 3D scanning water phantom (Blue Phantom/Wellhoefer (see Fig.3.1),Scanditronix/IBA Dosimetry group, Germany) was used. A small volume ionization chamber with a collection volume of 0.13 cm^3 , type CC13 and diode detector PFG^{3G}Photon for small field sizes (also Scanditronix/IBA dosimetry group) were fixed in the Blue Phantom. All data were proceeded with OmniPro-Accept software.

According to the requirements from the TPS supplier, for the commissioning of Monaco™ system following set of dosimetric data was required for all energies available: 6MV, 10MV and 18MV.

In water:

- PDD for at least 8 square fields, starting from smallest field size available (and physically consistent for measurements, i.e. 16x16 mm or 2x2 cm, respectively to MLC type) to maximum MLC field opening. Scans were performed to deepest obtainable depth in the phantom with the depth increment of 1 mm.
- PDD for at least 4 rectangular fields under the same conditions.
- In-line and cross-line profiles for all square and rectangular fields for the depths: d_{max} (depth of maximum dose), 5, 10 20 and 30 cm with the scan increment of 2 mm.

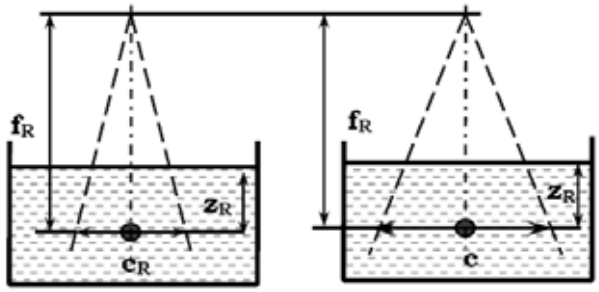

Figure 3.2: Output factor in a full scatter conditions

- Output factors for all square and rectangular fields at 100 cm SSD and 10 cm depth.
- Absolute dosimetry for 10x10 cm field at 10 cm depth.

In air (with the corresponding brass build-up cap for the chamber) for the same set of fields:

- Scan on central axis from 85 to 115 cm from the nominal focus of the photon source.
- In-line and cross-line scans for distances Z=85 cm, Z=100 cm and Z=115 cm from the nominal focus of the photon source.
- Relative output factors in air, normalized to largest field size.

Usually the measurements performed for the commissioning of the system should be done at the isocentric set-up, with the reference depth of 10 cm the reference distance of 100 cm. Beam data for the Monaco™ were required for 100 SSD, so the data measured before for the commissioning of other TPSs in the department couldn't be used. For all the fields output factors in air (head scatter factors) and in water (full scatter) need to be measured, as shown on the Fig. 3.2. Additionally film measurements were performed for reference field size at reference distance as well as transmission of the MLC leaves with polystyrene mini-phantom. All the data were than normalized for the output factors of a reference field size (10x10 cm) and absolute dosimetry measurements for the reference field size was performed in order to connect the linac output in MU to the dose (200 MU = 200 cGy).

For absolute dosimetry a cylindrical ionization chamber (PTW Freiburg, Germany) Farmer type 30001, volume 0.6 cc) positioned at 10 cm depth together with UNIDOS dosimeter (Fig.3.3)(also PTW) was used. The commissioning of the data and fitting to the Monte Carlo calculations were performed by CMS, St. Louis,USA.

3.1.2 Patient data acquisition

The output of three-dimensional treatment planning are doses in volumes of tissues rather than in individual planes. 3D information required to localize the tumor volume and normal

Figure 3.3: UNIDOS dosemeter and ionization chamber

tissues may be obtained from various imaging modalities. The patient's anatomical information commonly derived from CT or MR scanning. Also image fusion techniques with different imaging modalities such as PET, SPECT, MRI translated on CT scans are applied for better visualization of target volumes and OARs. The patient data are usually transferred to the TPS via DICOM-RT or DICOM 3 format.

To ensure correct dose calculation, the CT numbers (Hounsfield units, HU) need to be converted to electron densities and scattering powers. The conversion of CT numbers to electron density (cm^3) relative to water is usually performed with a look-up table provided by the manufacturer of the TPS. Although corrections for beam hardening etc. have been implemented in currently available CT scanners, a well-designed TPS should allow the user choosing or modifying the CT-to-ED (CT numbers to electron density) conversion file and/or additionally make possible the input of specific CT data sets measured in a phantom with different materials embedded. In contrast to analytical dose calculation algorithms, Monte-Carlo dose calculations are typically based on exact material composition and not on water equivalent properties. Thus a reliable CT-to-ED conversion of human tissues and IMRT verification phantoms should be obtained. The TPS Monaco™ provides a set of pre-installed CT-to-ED conversion files with customized calibration curves and the possibility of updating or exchanging these files.

Our aim was to determine the most appropriate conversion file for our planning CT (Siemens SOMATOM,Siemens AG, Germany) taking into account correct conversion of HU specific for human tissues and also for plastics used in IMRT verification phantoms. The CTP 404 module of the CATPHAN 504 phantom (The Phantom Laboratory, Salem, NY) is designed for monitoring of HU in CT images. It contains 1,2 cm diameter disks made of PMMA (acrylic), polystyrene, Teflon, air, etc. with different electron densities (see Fig.3.4).

By scanning the phantom for all CT imaging acquisition protocols to be used in a department, in particular, for IMRT treatment planning a mean curve of CT-to-ED conversion can be generated. The phantom underwent scanning under 3 different protocols used for potential IMRT patients (head-and-neck, thorax, abdomen-gynecological) and the data were transferred to the TPS XiO (CMS,USA) workstation for the absolute HU determination. HU were measured in 15 different points inside each material inserts and the mean values and standard deviations were obtained for each scanning protocol and compared with data provided by phantom

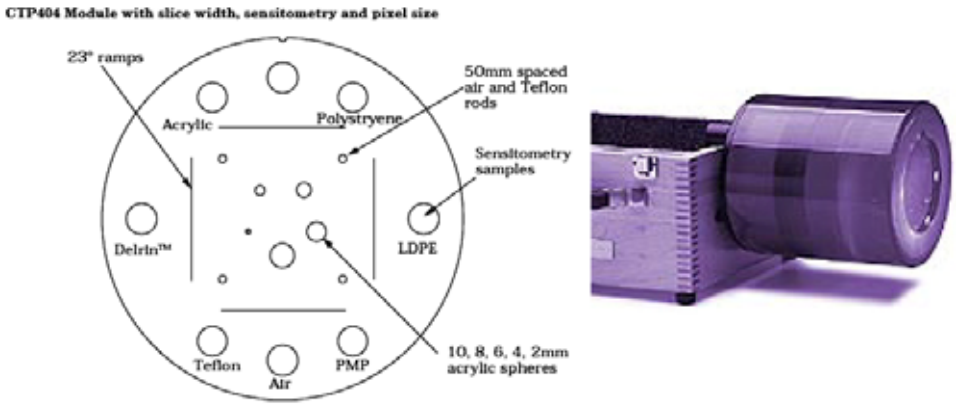

Figure 3.4: CATPHAN Phantom and sensitometric targets.

Material	Air	PMP	LDPE	Polystyrene	Acrylic	Delrin™	Teflon
Estim.HU	-1000	-200	-100	-35	120	340	990
Data acquisition protocol "Head"							
Mean HU	-1021.80	-214.27	-115.73	-50.43	125.53	373.87	1051.47
SD	1.47	6.34	4.04	5.05	3.18	11.84	9.02
Data acquisition protocol "Abdomen"							
Mean HU	-1014.40	-186.07	-98.87	-41.00	122.93	355.27	970.67
SD	10.06	5.86	5.28	6.86	4.54	11.68	14.73
Data acquisition protocol "Thorax"							
Mean HU	-1015.53	-185.47	-100.60	-39.93	117.67	354.80	964.87
SD	9.37	4.45	6.87	7.59	10.40	11.74	11.47

Table 3.1: Influence of different CT scanning protocols on HU determination.

manufacturer (Table 3.1).

HU accuracy for different materials and different scanning protocols satisfy limits of ±15 HU specified by IAEA for TPS (IAEA technical report [61]).

The adjustment of calibration curve for CT-to ED conversion is usually done by separation of high and low Z-ranges at a HU value between 100-150 and specifying a linear fit for each range, for instance, HU≤100 and HU>100. Different formulas for the relative electron density determination are reported in literature ([16, 67]).

For our calculations (see Table 3.2) we used method reported by Schneider [58], based on stochiometric calibrations from known chemical composition of 71 human tissues, whose characteristics were taken from literature. Following relationships (3.1 - 3.2) were used for the relative electron density calculations from the mean HU, defined in the phantom:

$$\rho_{el} = \frac{HU + 1000}{100} \qquad -1000 \leq HU \leq 47 \tag{3.1}$$

$$\rho_{el} = \frac{HU}{1827,15} + 1,0213 \qquad HU > 47 \tag{3.2}$$

	Acquisition protocol					
	"Head"		"Abdomen"		"Thorax"	
	HU	rel.e$^-$ dens.	HU	rel.e$^-$ dens.	HU	rel.e$^-$ dens.
Air	-1021.80	0.00	-1014.40	0.00	-1015,53	0.00
PMP	-214.27	0.79	-186.07	0.81	-185.47	0.81
LDPE	-115.73	0.88	-98.87	0.90	-100.60	0.90
Polystyrene	-50.40	0.95	-41.00	0.96	-39.93	0.96
Water	0.00	1.00	0.00	1.00	0.00	1.00
Acrylic	125.53	1.09	122.93	1.09	117.67	1.09
Delrin™	373.87	1.23	355.27	1.22	354.80	1.22
Teflon	1051.47	1.60	970.67	1.55	964.87	1.55

Table 3.2: Calculation of electron densities acc. to Schneider [58].

The data obtained were plotted together with the conversion functions given in Monaco™ (DICOM 3 legacy, DICOM 3 rocsboard etc.) and the conclusion about conversion accuracy was done (see Fig.3.5).

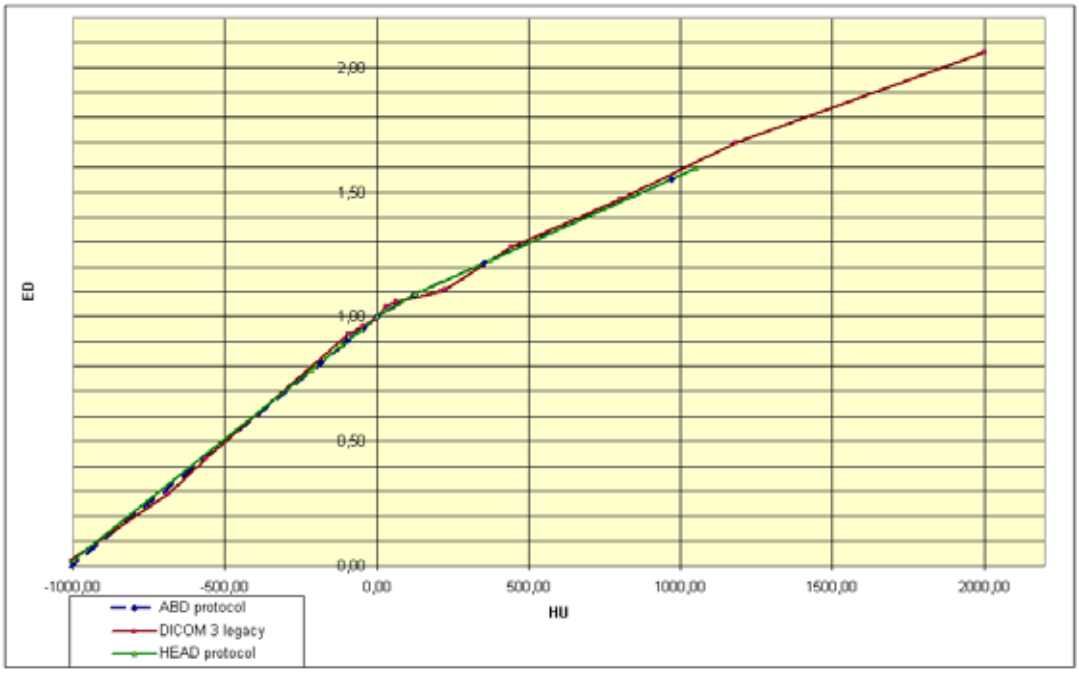

Figure 3.5: Comparison between DICOM 3 Legacy CT-to-ED conversion curve and data obtained from phantom measurements.

According to the results presented above necessary corrections were performed on the base of DICOM 3 legacy CT-to-ED conversion function and the following file denoted as DICOM 3

SIEMENS AKH was introduced into the Monaco™ (Table 3.3).

HU	ED
-1000	0
-773	0,19
-516	0,49
-200	0,8
-100	0,9
-72	0,95
-34	0,98
-4	0,99
0	1
42	1,04
49	1,05
120	1,09
238	1,12
360	1,22
951	1,51
1000	1,6

Table 3.3: DICOM 3 SIEMENS AKH conversion table.

The verification procedure of the CT-to-ED conversion allows defining CT-scanner specific deviations in HU determination and even preventing dosimetric inaccuracies [34]. Thus the adjustment of the conversion curves based on tissue-equivalent calculations with in-house phantom measurements improves accuracy of dose calculations [69] in dedicated phantoms.

3.2 Plan verification

After the commissioning of the intensity modulated radiotherapy treatment system and successful trials of system software for different planning approaches several plans, acceptable from the clinical point of view, were obtained (see patient case studies in chapter 4). Patient-specific IMRT verification is strongly recommended due to complex nature of the IMRT application process.

The procedure of so-called hybrid treatment plan verification was established and approved at the Medical University of Vienna [37]. It consists of several procedures. Firstly, it is single-point ionization chamber measurements to verify the number of MUs, followed by film measurements and quantitative dose verification procedure in dedicated phantoms. Secondly, it is independent MU verification with fluence-based verification software. New approach for IMRT verification with replacing EDR-2 films by Gafchromic EBT films was introduced and applied for the film measurements only recently.

Figure 3.6: Pelvic phantom for IMRT verification.

All IMRT plans were verified in a slab phantom designed to reflect shape of the body region (pelvis, can be used for thorax and head-and-neck verification)(see Fig.3.6). It is constructed from 3 cm thick plates of octogonal shape, made from polystyrene with a homogeneous density of 1.04 g/cm^3. The slabs are held together with two large laterally mounted screws, allowing to place and fix the position of the inserted films. This pelvic phantom has following dimensions: 35 cm width, 22.5 cm height, and it consists of 8 plates. In the centre of the phantom an insert is situated for the cylindrical Farmer type chamber NE 2611A (Nuclear Enterprise Technology Ltd, UK) with a sensitive volume of 0.325 cm^3. For measurements this ionization chamber is connected to a NE 2620 electrometer. The chamber is positioned at 10 cm depth at half distance between the two screws in order to enable measurements in the reference conditions i.e. at 10 cm depth.

In order to measure 2D dose distributions in axial planes and compare them with dose export files from the planning system, the chamber insert can be filled with polystyrene slabs and films can be placed then between vertical plates. More specifically, Gafchromic EBT films can be sandwiched between the plates and the isocenter position is marked with a help of needles fixed on three central phantom slabs. These marks are necessary for the accurate positioning of the reference point for quantitative evaluation of dose distributions.

The phantom was CT scanned and exported to Monaco™, where it was associated with the calculated patient study sets as a QA phantom. Patient plans were exported for the QA calculation procedure without changes in treatment geometry or any other treatment parameters. After re-calculation of the plan in a phantom (see Fig.3.7), plans were irradiated for the first time for the comparison of MUs computed for the phantom geometry with ionization chamber measurements. Than the chamber was replaced with three films (one in isocenter plane and the other 2at 3 cm distance in cranial and caudal direction). Dose files for the corresponding axial planes were exported from the TPS and exported to the software [64], where they were

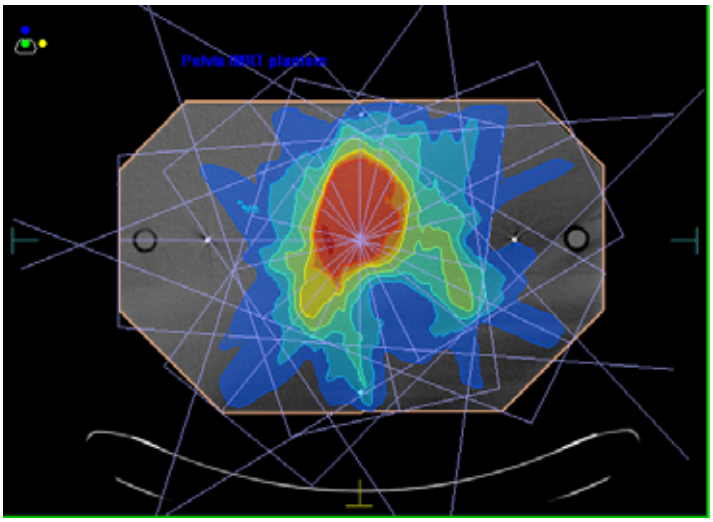

Figure 3.7: Recalculated on the pelvic phantom plan for the clinical case A (Chapter 3).

analyzed and compared with film measurements. In addition independent MU verification was performed in 5 points along the gantry rotation axis [29]. Calculated doses of the TPS and independent dose calculation were compared.

It is necessary to mention, that for ionization chamber measurements, as well as for independent MU verification procedure, in a case of a significant dose gradient the isocenter of the measurement point should be shifted. Homogeneous dose region is essential for the chamber positioning in order to obtain reliable results. Usually simple cranial-caudal transition of 1 cm is enough to reach a uniform dose region. The results of all verification procedures and some details on their procedure together with some theoretical background will be described in the following sections.

3.2.1 EBT film dosimetry

Especially for the evaluation of the calculated and measured the "ultimate" verification procedure should be well established and approved, because planned dose distribution contains the quality that has to be ensured and realized by QA activities. Silver-halide films have traditionally been used in radiation dosimetry, but because of their well-known disadvantages such as large differences in film sensitivity, need of special chemical procedure for film processing, non-tissue equivalent composition, the recently developed radiochromic EBT films are preferred.

Radiochromic films are self-developing and relatively insensitive for room light. The color of the film changes to dark-blue after radiation exposure and no post-exposure procedure is needed. They also have a tissue equivalent characteristics, ensuring low energy dependence in a measured range of energies. The radiochromic films currently available are the Gafchromic

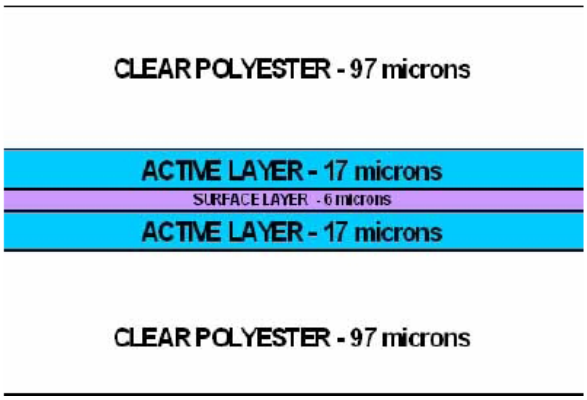

Figure 3.8: Structural composition of EBT film.

films produced by ISP (International Specialty Products, Wayne, NY) and their most recent type is the Gafchromic EBT film, which was launched in August 2004.

Film dosimetry equipment As specified by the manufacturer, the thickness of the EBT Gafchromic film is 0.234 mm and it consists of two active layers, each 17 μm thick covered by a surface layer of 3 μm. They are coated by a 97 μm clear, transparent polyester layer, as shown on the Fig. 3.8. The total film is formed by laminating the two pieces together without any intermediate adhesive layer. The atomic composition of the EBT film is the following: C (42,3%), H (39,7%), 0 (16,2%), N (1,1%), Li (0,3%), Cl (0,3%) with Z_{eff}=6.98, which is almost tissue-equivalent. The sensitive dose range for EBT dosimetry is between 0.01 and 8 Gy.

For radiochromic dose measurements a commercial scanner is used as a film reading device. At the Medical University of Vienna we use an EPSON Expression 1680 Pro scanner. This flatbed scanner is more user-friendly than for example the Vidar scanner and it has a good reproducibility. The software that comes together with the scanner is EPSON Scan - EPSON Expression 1680 Ver. 1.11E. When selecting the Professional Mode, the software gives the possibility to select various parameters. As we are scanning transparent films, the Document Type is set as "Transparency". Hence, we are measuring the optical density in transmission. For most of the experiment the Image Type is a 48-bit colour image (16 bit per colour: red, green and blue) that is saved as a RGB TIFF-file. This means the format throughout all experiments is the 48-bit TIFF-file, which is important because this format can be easily imported in MatLab and in the in-house developed dosimetric software. For the resolution we used 150 dpi, which was in most cases more than was required for our needs.

Evaluation of EBT films The detailed procedure of the evaluation of EBT films, their handling and calibration for the dosimetric measurements is provided in a literature [66]. Here only the essential information on measurement and evaluation procedure will be briefly described. The resulting TIFF-images from the scanning software are imported in a in-house

developed sofware "EBT-dose", executed in MatLab 6.5 (Math Works Inc., Natwick, MA). The scanner measures the transmission value per pixel and per colour channel (red, green or blue), further referred to as the pixelvalue. These pixelvalues can be easily converted by the software into optical densities, with the following transformation 3.3:

$$OD = \log 10(\frac{2^{16}}{pv + 1}) \tag{3.3}$$

The "EBT-dose" software besides the calculation of the optical density, also performs the correction of measured pixelvalues with reference to their position on the scanning plate. That is essential, because for IMRT verification the whole film sheet is used and the deviations depending on the film position on the scanning plate should be eliminated.

In order to exclude influence of the scanner inhomogeneities a correction matrix is necessary. For the correction matrix the scanning plate was divided into squares with area of 2 cm^2 (40x40 pixels) and a piece of a film was scanned in each position. The deviation in optical density between the centre of the scanning bed and other positions was determined and introduced into the correction matrix, which is applied by the evaluation software to every scanned film.

All measurements were performed on the data in the red channel, because the after scanning of irradiated film, the maximum absorption peak lies at 636 nm. Also the red channel has the biggest dynamic range, less noise and better reproducibility and stability of measurements. The use of the red channel is also recommended by manufacturer and other references [52, 53].

After the correction of the film positioning and choosing the color channel, for every new series of films (packs with the same serial number), the calibration curve should be introduced into "EBT-dose" software. The calibration curve represents the dependence of net optical density (measured vs background scan) versus applied dose. The data points were fitted by a 4th grade polynom. The pieces of the EBT film (3x3 cm, ROI - 2 cm^2) were irradiated with doses from 20 cGy to 400 cGy, and the net optical density was determined and introduced into software. Based on this calibration not only relative dose values but also absolute dosimetry can be performed with "EBT-dose", but the uncertainty in absolute dose determination is limited to around 5%.

Finally, the "EBT-dose" software allows to import dosimetric information in ASCII format for further evaluation. The protocol for EBT dosimetry, used for IMRT plan verification was the following:

EPSON scanner protocol:

- Heat-up the scanner by 6 successive scans prior to measurements.
- Use the positioning frame for the reproducibility of a film position
- Perform always two scans for the background and irradiated films, where only the second will be used for measurements.

- Use always the same specifications in the EPSON software (professional mode, transparent document type, 48-bit, colour correction off, 72-150 dpi, scanned area: max 1064x1500 pixel).

EBT film protocol:

- Use gloves to handle the film.
- Store non-irradiated films in a dark place.
- Cut films, if necessary, minimum 1 day prior to irradiation (because pressure causes temporal changes in a film structure).
- Use the films in portrait orientation for scanning (there is an impact of scanning orientation on the optical density determination due to internal structure of a polymer).
- Make a background scan of the films before irradiation in order to compute the net optical density values.
- After irradiation, wait at least 6 hours to scan the films.
- Use EBT-dose software to obtain and proceed the measured pixelvalues.

3.2.2 γ - evaluation method

The computed or planned dose distribution often serves as the gold standard in QA. Therefore, the comparison of the evaluated dose distribution with the planned distribution is essential. There are different methods to make this comparison of two-dimensional dose distributions, but currently the commonly accepted and adapted approach is the γ evaluation method, proposed by Low et al [42].

In fact, it is a generalization of the traditional concepts, where Figure (3.9) gives a graphical overview of the geometrical basics and terminology. The parameters for evaluation are the dose difference ΔD_M between measured and calculated doses in a certain point and the "distance-to-agreement" or DTA (Δd_M), which is the distance between a measured data point and the nearest point in the calculated dose distribution that has the same dose. Usual criteria are 3 mm for the DTA and 3% (of the dose in the normalization point) for the dose difference. The measured dose is here used as reference and the calculated distribution is the one that gets compared to it.

Fig.3.9 illustrates an evaluation for a single measurement point $\vec{r_m}$, lying at the origin of the figure. The δ-axis represents the difference between the measured dose$[D_m(\vec{r_m})]$ and the calculated dose $[D_c(\vec{r_c})]$. The x- and y-axis reprecent the spatial location $\vec{r_c}$ for the calculated distribution relative to a measured point.

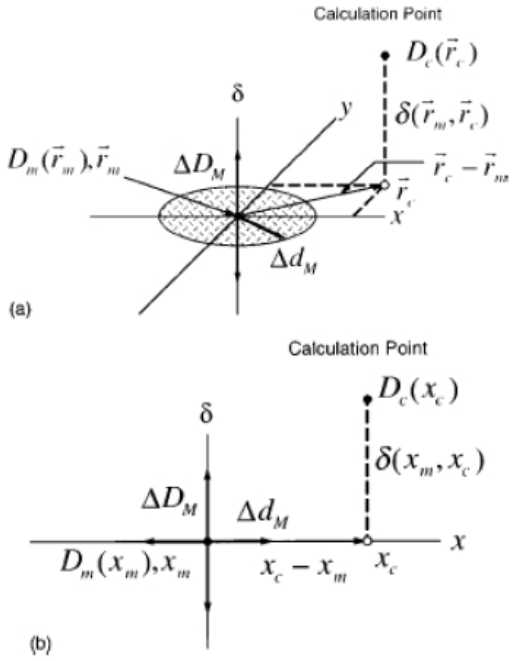

Figure 3.9: Geometric representation of dose distribution evaluation criteria for the dose difference and DTA tests; (a) two-dimensional representation, (b) analogue one-dimensional representation [42].

The vertical line with a length of $2\Delta D_M$ represents the dose difference test. If the calculated dose distribution surface crosses the line $[D_c(\vec{r_m}) - D_m(\vec{r_m}) < \Delta D_M]$, the calculated distribution passes the dose difference test at the measurement point $\vec{r_m}$.

The DTA criterion, Δd_M, is represented by a disk in the $\vec{r_m} - \vec{r_c}$-plane with a radius of Δd_M. If the calculated dose distribution surface, $D_c(\vec{r_c})$, intersects the disk, the DTA is within the acceptance criterion and the calculated dose distribution passes the DTA-test for that point.

The γ-index concept Defining the acceptance criteria not just along the δ-axis and in the $\vec{r_m} - \vec{r_c}$-plane allows a more general comparison between calculations and measurements than the traditional composite evaluation does. Thus an ellipsoid is constructed as the surface defining the new criterion. The equation that defines this surface is:

$$\sqrt{\frac{r^2(\vec{r_m},\vec{r_c})}{\Delta d_M^2} + \frac{\delta^2(\vec{r_m},\vec{r_c})}{\Delta D_m^2}} = 1 \tag{3.4}$$

with the distance between the measured and the calculated dose

$$r(\vec{r_m},\vec{r_c}) = |\vec{r_c} - \vec{r_m}| \tag{3.5}$$

and the dose difference at point $\vec{r_m}$

$$\delta(\vec{r_m},\vec{r_c}) = D_c(\vec{r_c}) - D_m(\vec{r_m}) \tag{3.6}$$

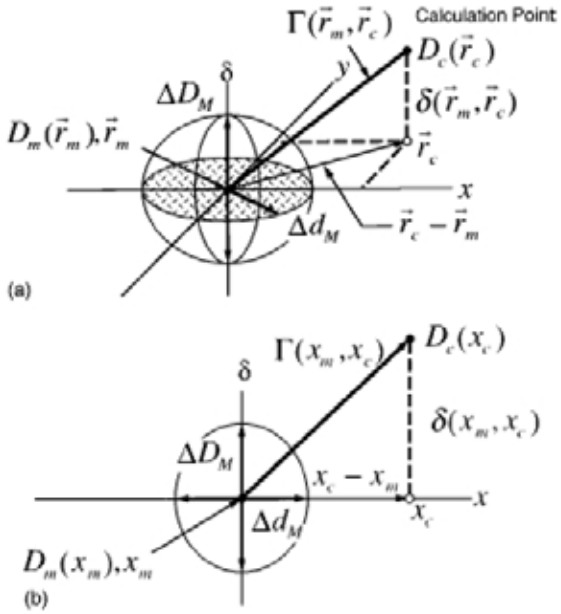

Figure 3.10: Geometric representation of dose distribution evaluation criteria using the combined for the dose-difference and DTA test; (a) two-dimensional representation, (b) analogue one-dimensional representation [42].

If any portion of the calculated dose distribution surface $[D_c(\vec{r_c})]$ intersects the ellipsoid, the defined criterion is fulfilled at $\vec{r_m}$. Based on this terminology, the γ-index, which is the minimum distance between the measurement point under investigation and all points of the calculated distribution, is calculated as follows:

$$\gamma(\vec{r_m}) = min\,\{\Gamma(\vec{r_m}, \vec{r_c})\}\,\forall\,\{\vec{r_c}\} \tag{3.7}$$

with

$$\Gamma(\vec{r_m}, \vec{r_c}) = \sqrt{\frac{r^2(\vec{r_m}, \vec{r_c})}{\Delta d_M^2} + \frac{\delta^2(\vec{r_m}, \vec{r_c})}{\Delta D_m^2}} \tag{3.8}$$

The ellipsoid represents the surface of the combined acceptance criteria (see Fig.3.10). Mathematically it can be expressed as

$$\gamma(\vec{r_m}) \leq 1 \tag{3.9}$$

Next to the γ-index, also the γ-angle is considered to be a very useful tool for the interpretation of dose distributions. The γ-angle indicates the parameter mostly influencing the γ-index, the dose difference or the DTA. If the γ-angle is between 0 and $\pi/4$ the γ-index is dominated by the dose difference, if it lies between $\pi/4$ and $\pi/2$ the γ-index is dominated by the DTA. The angle is calculated with the absolute values of dose difference and distance difference; thus the γ-angle is always between 0 and $\pi/2$.

For a comfortable evaluation, it is preferable to graphically display the γ-index distribution as well as the γ-angle distribution. In addition, it is possible to statistically evaluate the γ-

values by means of histograms. Both features are implemented in the program described in the following section.

The Dos-Ver software The software package "DosVer"(Dosis Verifikation) provides a fast generation of γ-index distributions due to an optimized calculation algorithm. The program and its mathematical functionalities are described in detail in the diploma thesis of Stock (2003) [64], who has developed the software at the Medical University of Vienna. In the following only the main features and highlights of the program will be presented. As an example, the verification procedure of the head-and-neck case described as "Case study B" in chapter 4, which was performed in the IMRT verification phantom, is discussed.

First of all, the software needs the measured and calculated dose distributions as input data. The "EBT-dose" software exports the relative dose distribution as a text-file, which can directly be imported into the "DosVer" program. The TPS Monaco™ provides calculated dose distributions in any plane of interest as a text-file. The definition of following parameters as isocenter position and normalization point in both dose distributions, is the required next step. The absolute dose delivered to the normalization point (100%) and the pixel resolution (pixel spacing should be equal in both files) are needed to run the program. We use a dose matrices of 1 mm pixel size, which is one third of the DTA criterion and provides avoidance of the artefacts in γ-index calculation. As a third step, the user has to define a region of interest (ROI), which should exclude needle marks on the films but also be sufficiently large for an

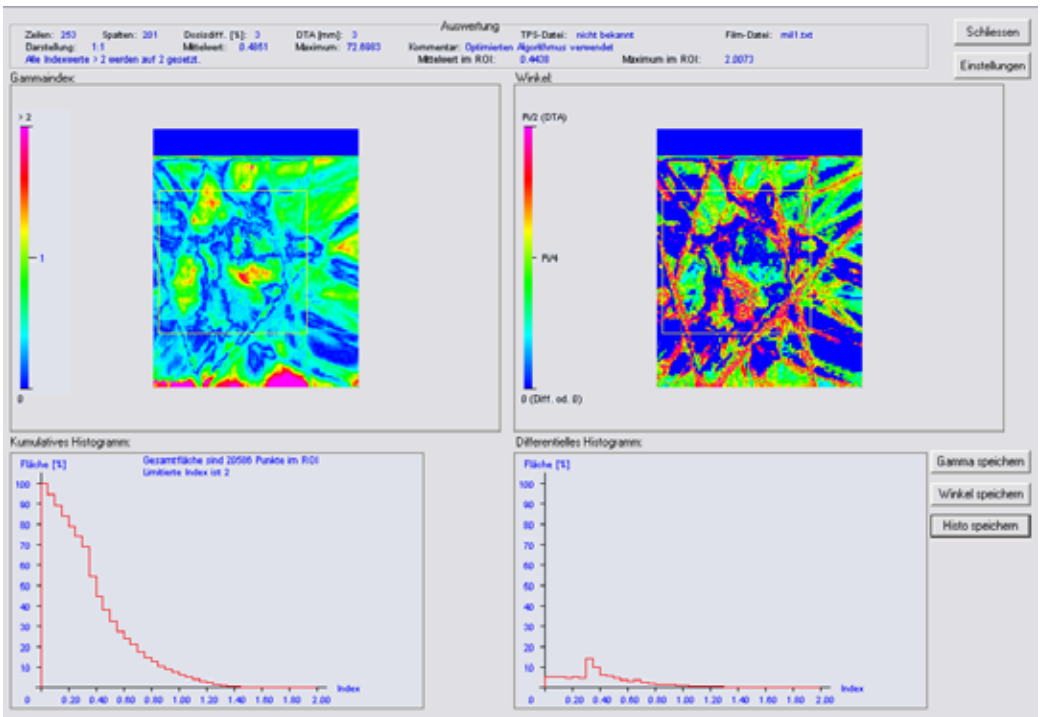

Figure 3.11: Results of the γ-index analysis in "DosVer" software .

objective evaluation. After the input of the data from film and TPS the software displays dose difference map between the measured and calculated distribution, which primarily helps to detect geometrical misalignment between the two data sets. As expected, the highest dose differences are found along the steep dose gradients at the field edges. Another useful tool to detect geometrical misalignment more precisely is a comparison of the row and column dose profiles.

The procedure of γ calculation takes only around 30 seconds for a 20x20 cm large film at 1 mm pixel resolution. As an example, results are shown in Figure 3.11. In the upper left chart, γ-index values are graphically displayed. While the predefined blue and green areas indicate good agreement between the dose distributions within the requested acceptance criteria (3% and 3 mm), the yellow and red regions represent points of violation. Again, the yellow rectangle delineates the ROI, for which the mean γ-value is calculated. In the upper right part the γ-angle distribution is illustrated. In the lower part of Figure 3.11, cumulative (left) and differential (right) γ-area-histograms are shown. The information about the number of points exceeding the acceptance criteria can be proceeded in a form of a table from these histograms.

Acceptance criteria During the last years an evaluation filter for hybrid plan verification was established at the Medical University of Vienna in 2004 [65], which is represented in the table 3.4.

Parameter	Range	Appraisal and approach
$\gamma_{1\%}$	0 - 1,5	Acceptable
	1,5 - 2	Acceptable, but other verification tools like angle distribution,dose difference map and profiles needed for further evaluation
	>2	Measurement has to be repeated - if violation remains, treatment plan has to be re-optimized
γ_{mean}	0 - 0,5	Acceptable
	0,5 - 0,6	Acceptable, but other verification tools like angle distribution,dose difference map and profiles needed for further evaluation
	>0,6	Measurement has to be repeated - if violation remains, treatment plan has to be re-optimized
area with γ >1	0 - 5%	Acceptable
	5 - 10%	Acceptable, but other verification tools like angle distribution,dose difference map and profiles needed for further evaluation
	>10%	Measurement has to be repeated - if violation remains, treatment plan has to be re-optimized

Table 3.4: Evaluation criteria for IMRT treatment plans based on the γ-index.

Surely, this filter can be equipment-dependent and it is valid for the 3% and 3 mm acceptance criteria.

3.2.3 MU verification

Independent dose calculation techniques are useful for patient-specific IMRT verification and represent a good alternative to experimental methods. As a general requirement for verification dose calculation software is that:

- the basic beam data,
- dose calculation algorithm,
- software implementation

need to be as independent as possible from the treatment planning system, and should be based on physical effects that can be "tuned" for each accelerator by a set of input data. An MU software should be designed with a high degree of accuracy, including the estimation of the overall uncertainty in the dose calculation.

The accuracy and performance of the MatLab-based independent dose calculation software MUV (monitor unit verification) was recently published by Georg at al. [29,30]. This software is used in clinical routine at the Department of Radiotherapy, Medical University of Vienna.

The semi-analytical model of the MUV software is based on two components: first the energy fluence per MU exiting the treatment head and, secondly, calculation of the dose deposition in the phantom due to the energy fluence from the previous step. The fluence deposition takes into account the direct energy fluence, scattered radiation from extra-focal source, backscattered radiation from the collimators and effects in collimator transmission, tongue-and-groove effect and leaf leakage. The dose deposition calculation is based on the pencil beam model.

A DICOM interface allows importing of the dosimetric and geometric treatment data for a treatment plan simultaneously and the set of data for an independent calculation (MU per segment, leaf and collimator settings, energy and position of a dose specification point) is transferred directly from the TPS. The final result of the dose calculation with MUV software is the dose to water in a pre-defined point in a verification phantom, for a composite treatment plan or for an individual beam. The point of interest in the patient can be modified in all directions in MUV by the user, so that finally multiple points can be verified if needed.

In the Department of Radiotherapy, Medical University of Vienna, IMRT QA with MUV software is based on the dose calculation for minimum of 5 points, including the isocenter (if no steep dose gradient takes place there) and other 4 points along the gantry rotation axes. The calculation of the dose in these points, including the export of the plan, data analysis and documentation, takes around 20 min only, which is ten times less than verification by experimental approach.

Based on the results of the benchmark study [29], the following confidence limit was proposed: 3% dose deviation (with respect to the prescribed dose) or 6cGy for full IMRT plans and individual points close to isocentre. The points usually cover the high dose regions in the PTV(s), dose region with 70%-50% of the prescribed dose outside the target, as well as the low dose region.

The results of the independent dose calculation for 6 IMRT plans calculated with MUV and the comparison with the dose calculated by Monaco™ together with the experimental verification will be presented in the next section.

3.2.4 Hybrid plan verification results

For the verification of Monaco™, six plans of different complexity and calculated with different algorithms were taken. One plan was done head-and-neck case with 50 Gy prescription for all

target volumes, the second for head-and-neck case with 2 dose levels (case B in Chapter 4). Two plans were created for head-and-neck case with 3 dose levels (case A in Chapter 4), calculated and optimized with the FSPB and Monte Carlo algorithms, respectively. Additionally plan for gynecological case (case C in Chapter 3) was included into the study.

Firstly all plans were verified with the MUV software, then EBT film measurements were performed and the dose in all isocenter points was also verified by ionisation chamber measurements.

The output for 10x10 reference field was 201,3 and 203,4 MU for 2 Gy at 10 cm depth in a polystyrene phantom for pencil beam and Monte Carlo calculations respectively. The verification of the dose in the isocenter point (or 2cm in cranial direction, if the isocenter is close to the dose gradient) showed the following results:

Plan	Point	Chamber value	TPS value	Deviation
1	2 cm cranial	1,88	1,92	-1,6%
2	2 cm cranial	1,95	1,987	- 1,9%
3	ISO	1,82	1,85	-1,6%
4	ISO	1,83	1,86	-1,3%
5 MC	2 cm cranial	1,89	1,95	-2,8%
6 MC	2 cm cranial	1,80	1,82	-1,1%

Table 3.5: Ionisation chamber measurements compared to TPS calculated dose

The results of the γ-index verification for all the plans is presented in the table 3.6.

Plan	γ_{mean}	area with $\gamma > 1$	$\gamma_{1\%}$
Plan 1	0,47	7,7%	1,68
Plan 2	0,48	6,9%	1,61
Plan 3	0,39	5,1%	1,35
Plan 4	0,34	4,7%	1,29
Plan 5 MC	0,46	8,1%	1,85
Plan 6 MC	0,32	5,5%	1,61

Table 3.6: Verification results for IMRT treatment plans by γ-index criteria.

All points taken for MUV verification have passed acceptance criteria of 3% deviation. The mean value for the dose deviation between MUV and TPS was $-0,82 \pm 1,3(SD)$ for pencil beam calculations and $1,14 \pm 0,51(SD)$ for Monte Carlo calculations. The results of the verification are presented in the table below (Table 3.7). It is necessary to mention that all techniques are influenced by linac stability and positioning accuracy of MLC.

	Point	MUV value (Gy)	Monaco value(Gy)	Deviation (%)
			MUV verification	
			for pencil beam calculations	
Plan 1	1	2,016	1,987	-1,4
	2	2,102	2,089	-0,6
	3	2,153	2,189	1,6
	4	1,678	1,664	-2,0
	5	1,705	1,692	-0,6
Plan 2	1	1,940	1,897	-2,2
	2	1,888	1,848	-2,1
	3	1,951	1,908	-2,2
	4	1,935	1,917	-0,9
	5	1,921	1,916	-0,2
Plan 3	1	1,90	1,857	-2,4
	2	1,861	1,872	0,5
	3	1,571	1,534	-2,2
	4	1,584	1,582	-1,9
	5	1,861	1,861	0,0
Plan 4	1	1,946	1,913	-1,7
	2	1,913	1,922	0,4
	3	1,903	1,942	2,0
	4	1,832	1,809	-1,2
	5	1,812	1,807	-0,2
			MUV verification	
			for Monte Carlo calculations	
Plan 5	1	1,853	1,879	1,3
	2	1,946	1,961	0,7
	3	1,985	2,014	1,1
	4	1,636	1,656	1,2
	5	1,620	1,634	0,8
Plan 6	1	1,683	1,708	1,4
	2	1,880	1,879	-0,1
	3	1,881	1,908	1,4
	4	1,854	1,877	1,2
	5	1,891	1,850	1,7

Table 3.7: MUV verification results

Chapter 4

IMRT treatment planning studies

4.1 Clinical application of IMRT

There are the major clinical sites, that have been explored during the past decade [9]:

- Head-and-neck IMRT (paranasal, sino-nasal tumors, carcinomas of the oropharynx and oral cavity, carcinomas of the nasopharynx);
- Paraspinal tumors;
- Breast IMRT;
- Lung IMRT;
- Prostate IMRT;
- Malignancies of the upper abdomen;
- Gynecological IMRT (carcinomas of the uterine cervix and endometrium).

All these diffrent applications of IMRT have different degrees of success and choice is based on clinical, physical and economical considerations of an institution.

In Department of Radiotherapy, Medical University of Vienna IMRT is mostly applied for treatment of the carcinomas of naso- and oropharynx (here the benefit of choosing IMRT over conformal techniques can't be doubted) and cervical carcinomas. Therefore, in this chapter studies focus on these applications.

All cases were planned for delivery on Elekta Synergy Platform linear accelerator with MLCi (Elekta, Crawley,UK) with energy 10 MV. Dose calculation and optimization was performed

firstly on a 4 mm grid size with FSPB algorithm and the Monte-Carlo algorithm was employed for dose calculation and optimization of head-and-neck cases A and B.

4.1.1 Clinical case A (head-and-neck)

IMRT has been recommended in the treatment of head and neck cancer, given the close proximity of critical organs such as the spinal cord, brain stem and salivary glands, the risk of exposing of exposing the patient to acute and/or delayed and sometimes severe complications. The main expected advantage concerns the dose reduction to the parotid glands, resulting in decreased incidence of xerostomia [18, 40, 76]. The loss of salivary output is a major complication because it leads to a dry mouth, difficulty in swallowing, impairment of food tasting and deterioration of dental health.

IMRT patients are simulated and treated in aquaplast mask, which provide better positional accuracy. Planning CT was performed with 2 mm slice thickness and the international guidelines were used to define CTV [31]. The usual OARs were contralateral parotid gland, spinal cord, brainstem and larynx. The CTV's were expanded isotropically by 5mm to account for patient setup and motion to obtain the PTVs.

The PTV dose prescription for definitive or postoperative radiotherapy varied from 50 to 70 Gy, using a so-called SIB technique. Dose prescriptions to OARs were as follows: $D_{mean} \leq 26$ Gy for parotid gland, $D_{max} \leq 45$ Gy for spinal cord $D_{max} \leq 49$ for brainstem.

For this case the prescribed doses were from 50 to 70 Gy in 31 fractions, so we had the dose range from 1,61 to 2,26 Gy (boost) per fraction for different PTVs. Following 7 beam arrangement was chosen: $39° - 90° - 141° - 193° - 244° - 296° - 347°$. One beam (in this case gantry angle at 90 degrees) goes through parotid gland which we want to spare, this beam positioning was found as the most convenient for this purpose [63].

An isotropic 5 mm margin was applied to all CTV's in order to construct 4 PTVs for the different dose levels (70 Gy for the primary tumor, 60 Gy on ipsilateral lymph nodes level I-III, 50 Gy on level IV ipsilateral and contralateral lymph nodes). As OARs we outlined spinal cord, brain stem and contralateral parotid gland (see Fig.4.1).

These structures were used for optimization. The prescription in Monaco™ included 8 structures: all 4 PTVs, spinal cord, brain stem, left parotid and external contour (Body). Three cost functions were assigned to PTV 70 Gy:

- **Poisson Cell Kill Model** with an iso-constraint of 73,5 Gy (in order to prevent the loss of PTV coverage during the segmented optimization)
- **Quadratic Overdose Penalty** constraint with reference dose of 73,5 Gy and 2 Gy RMS limit.

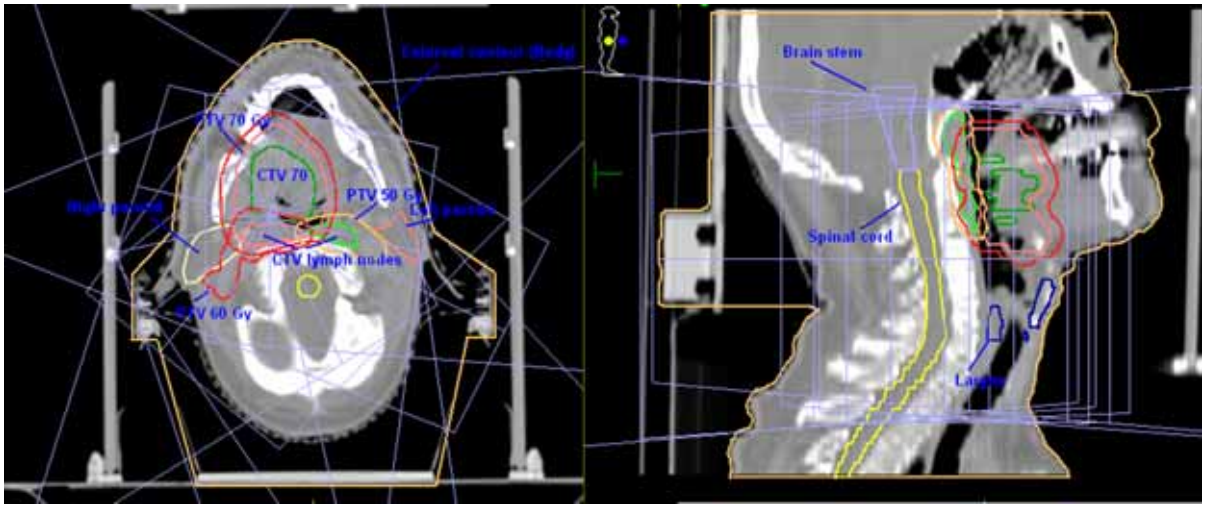

Figure 4.1: Target volumes and OARs delineation for the case A.

- **Maximum Dose Constraint** with iso-constraint value of 79,5 Gy in order to prevent any dose higher than 115% of the prescribed dose.

Two cost functions were assigned to PTV 60 Gy (lymph nodes level I-II on the right side):

- **Poisson Cell Kill Model** with iso-constraint of 63 Gy.
- **Quadratic Overdose Penalty** constraint with reference dose of 63,5 Gy and 2 Gy RMS limit.

For PTV's 50 Gy the same cost functions as for PTV 60 were given: **Poisson Cell Kill Model** with iso-constraints of 54 Gy and 52,5 Gy and **Quadratic Overdose Penalty** constraint with reference doses of 55 Gy and 54 Gy and RMS limits 2,5 Gy for right and left sides respectively.

For the spinal cord the **Serial Complication Model** cost function was assigned with an EUD value of 29,5 Gy and a power law exponent $k = 10$, together with the option "Optimize over all voxels in a volume" turned on. This option allows to apply the constraint for all voxels even partly included in a structure or overlapped with other structures. For the brain stem also the **Serial Complication Model** cost function was assigned with an EUD of 31 Gy and a power law exponent $k = 10$.

The **Parallel Complication Model** cost function was taken for the optimization of the dose to the parotid gland with the reference dose of 24 Gy, power law exponent equal 3 and Mean Organ Damage of 31%.

Also the additional constraints for normal tissue were introduced for optimization process in order to exclude possible hot spots in larynx or other regions. Prescribed doses to the Body were specified with two **Quadratic Overdose Penalty** constraints: first with the reference dose of 48,5 Gy and a RMS dose excess of 2 Gy, and second with the reference dose of 35 Gy

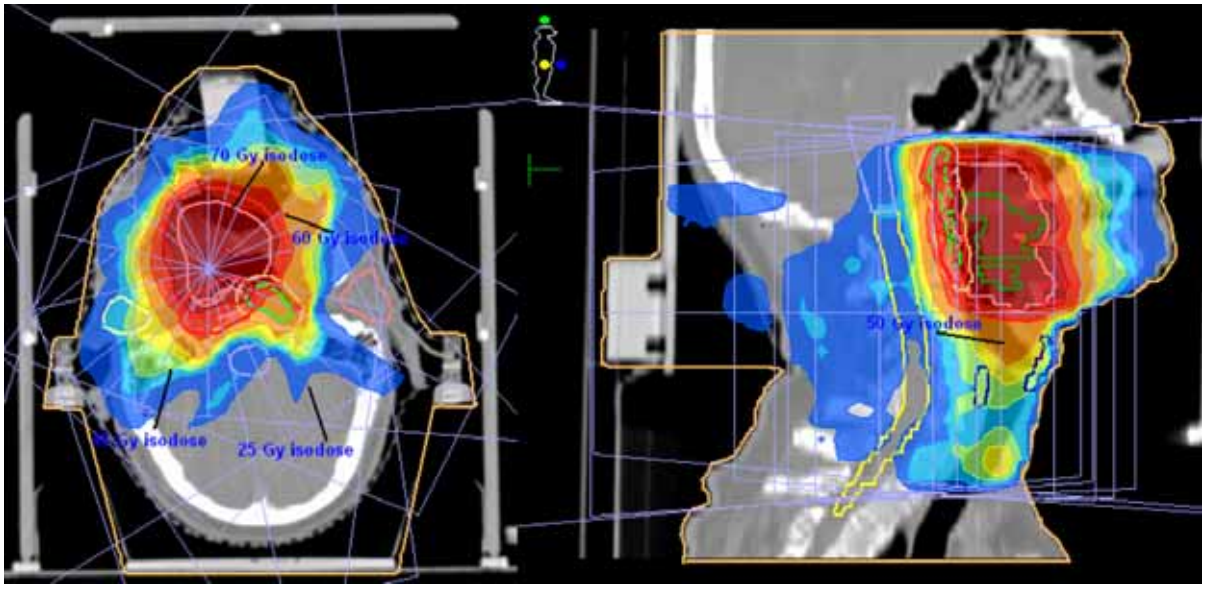

Figure 4.2: Dose distribution on the axial slice for the case A.

and a RMS limit of 1,5 Gy was applied to the area of the structure 2 cm away from the target volumes ("Shrink Margin" option). The dose distribution is presented in the Fig.4.2.

The plan was compared with optimization results from the TPS Oncentra MasterPlan (Nucletron, NL) which is currently used in clinical routine. The comparison of results obtained with Monaco™ and Oncentra Masterplan, together with the DVHs for targets and OARs are given below (Table 4.1 and Fig. 4.3, 4.4).

		OMP optimized	Monaco optimized
PTV coverage	PTV 70Gy	98%	97,5%
with 95% of D_{prescr}	PTV 60Gy	98%	99%
	PTV 50Gy right	97%	99,5%
	PTV 50Gy left	97%	99,1%
Mean dose to parotid		26,1 Gy	24,2 Gy
Max dose to spinal cord		45,7 Gy	36,3 Gy
Max dose to brain stem		48,1 Gy	40,2 Gy
Absolute Max dose		76,7 Gy (113%)	76,9 Gy (109%)
Number of segments/MU		98/498	93/864

Table 4.1: Plan evaluation results from OMP (DVH-based optimization) and Monaco (biologically constrained optimization).

Also this case was re-optimized with the dose calculation on Monte Carlo module. It was necessary in order to see the difference in the obtained dose distributions (constraints are the same as for FSPB optimization). After a Monte Carlo based optimization in Monaco™ the

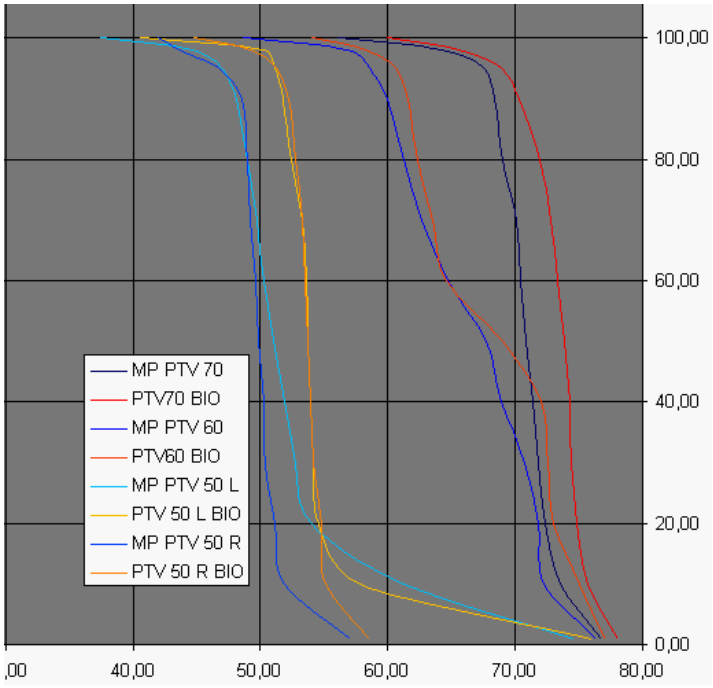

Figure 4.3: DVH comparison for target volume (dark blue, blue and light blue lines - Oncentra MasterPlan, dark red, red and orange lines - Monaco optimization results).

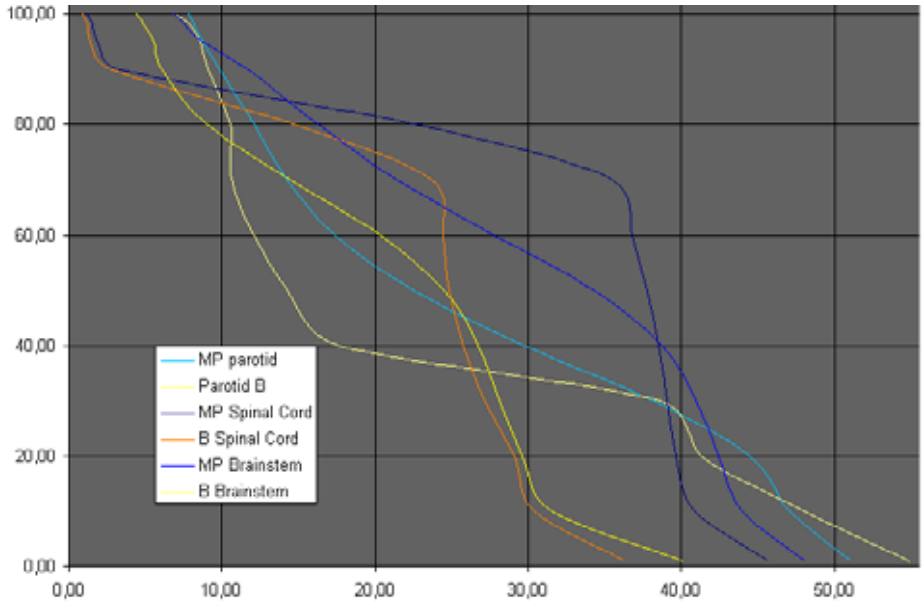

Figure 4.4: DVH comparison for OARs (dark blue, blue and light blue lines - Oncentra MasterPlan, orange, yellow and light yellow lines - Monaco optimization results.)

number of segments was 80 with a total of 1090 MU. The Fig.4.5 presents the dose difference between plans optimized with FSPB and Monte Carlo algorithms, respectively.

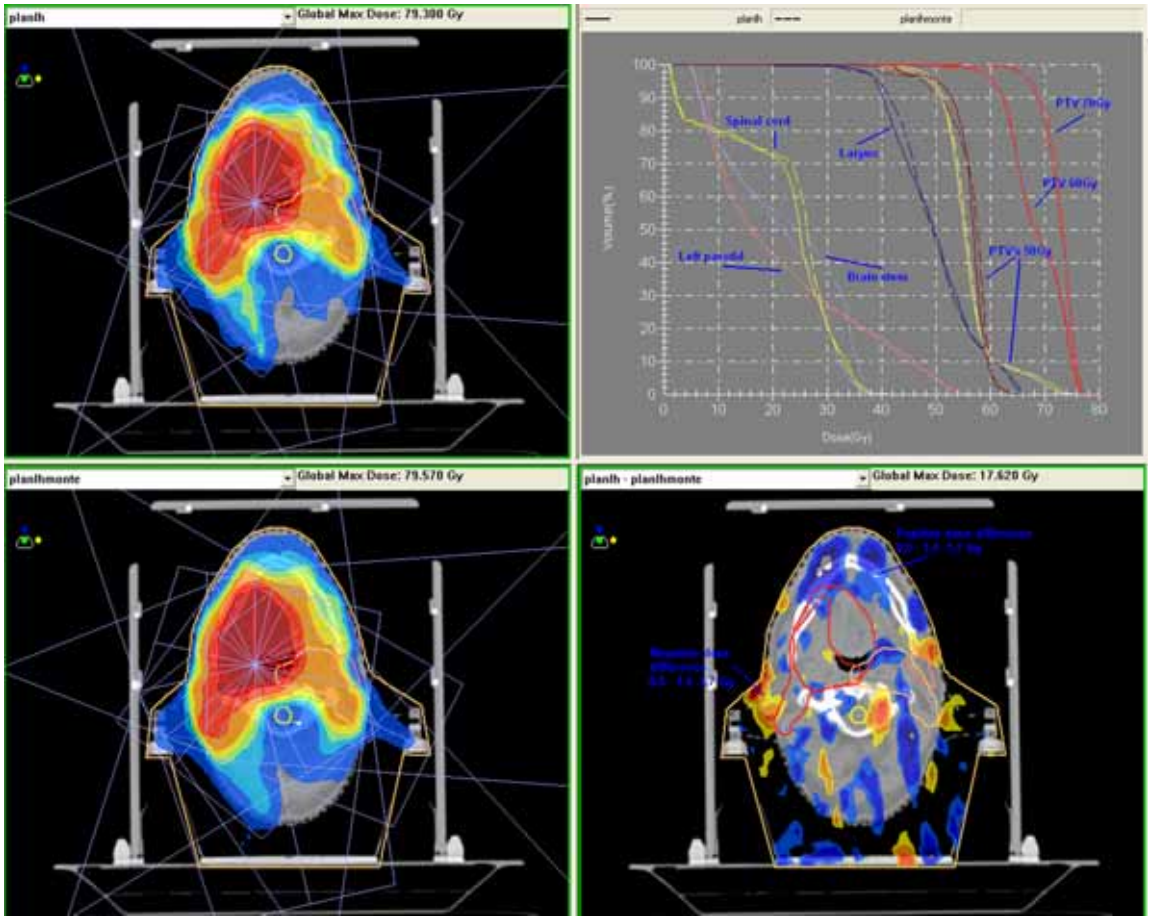

Figure 4.5: Comparison of the DVHs and dose distributions for FSPB and Monte Carlo optimized plans.

After the further implementation of more strict conditions on the cost functions, such as increasing of a power law exponent and reducing an EUD for all OARs, following results were achieved:

- PTV coverage: **96,6- 98,2%** for different PTVs,
- Absolute maximum dose: **79,56/113%** Gy,
- Max dose to brain stem: **39,17** Gy,
- Max dose to spinal cord: **40,8** Gy,
- Mean dose to parotid gland: **21,6** Gy.

In this case, number of segments was 86 with a total of 1060 MU.

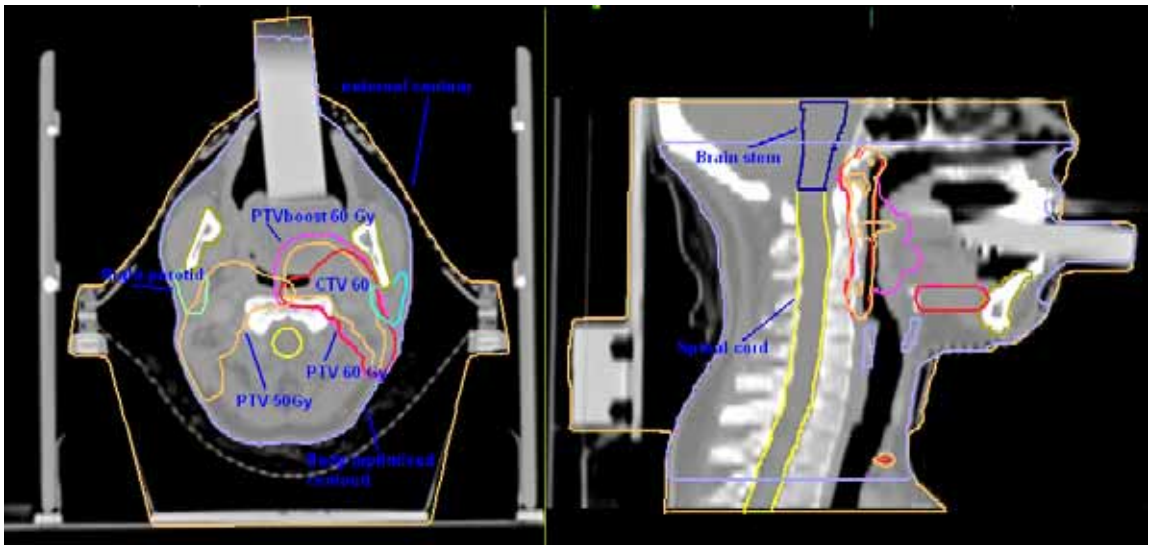

Figure 4.6: Target volumes and OARs delineation for head-and neck case B.

4.1.2 Clinical case B (head-and-neck)

For case B the prescribed doses were 50 Gy to the lymph nodes and 60 Gy boost to the tumor, delivered in 30 fractions. The same 7 beams arrangement as for the case A was applied, but rotated around 180 degrees (because in this case the contralateral parotid gland is on the right side). A 5 mm isotropic margin was applied to all CTV's in order to construct PTVs for the different dose levels. As following OARs we outlined and used for optimization spinal cord, brain stem and contralateral parotid gland (see Fig.4.6).

The prescription included 7 structures: 3 PTVs (60 Gy, 50 Gy on contralateral and ipsilateral lymph nodes), right parotid gland, spinal cord, brain stem and external contour (Body). Three cost functions were assigned to PTV 60:

- **Poisson Cell Kill Model** with an iso-constraint of 63 Gy,
- **Quadratic Overdose Penalty** constraint with reference dose of 64 Gy and 2 Gy RMS limit.
- **Maximum Dose Constraint** with an iso-constraint value of 68,8 Gy.

To PTVs of 50 Gy were assigned 2 cost functions:

- **Poisson Cell Kill Model** with an iso-constraint of 53/54 Gy for the left and right side, respectively.
- **Quadratic Overdose Penalty** constraint with reference doses of 54/53,5 Gy and 2/1,5 Gy RMS limit for the left and right side respectively.

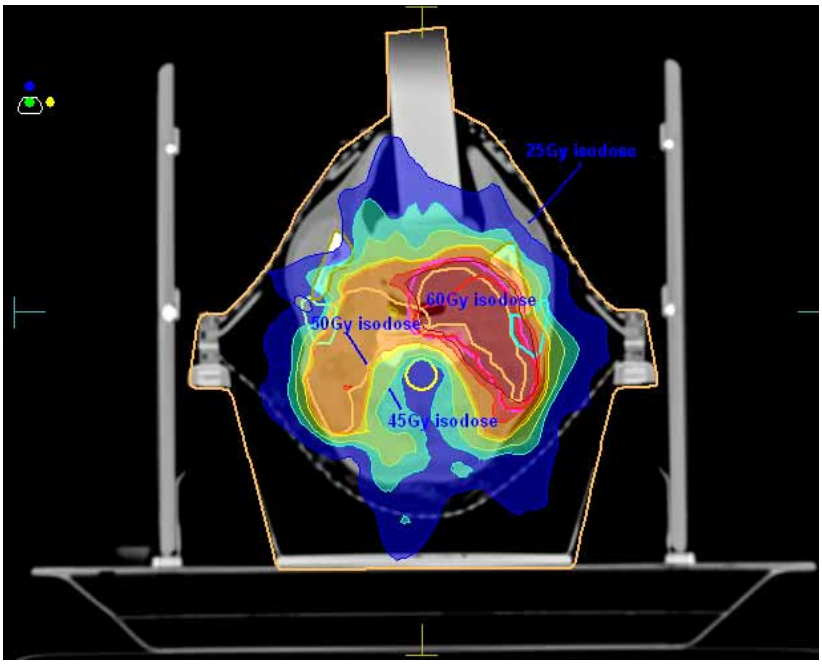

Figure 4.7: Target volumes and OARs delineation for gynecological case.

The **Serial Complication Model** cost function was assigned to the spinal cord with an EUD value of 31 Gy and a power law exponent $k = 13$. The option "Optimize over all voxels in a volume" turned on. The larger power law exponent implies a higher penalty on constraint violation. For the brain stem also the **Serial Complication Model** cost function was assigned, with an EUD of 34 Gy and a power law exponent $k = 10$.

The **Parallel Complication Model** cost function was taken for the optimization of the dose to the parotid gland with the reference dose of 25 Gy, power law exponent was set to 3 with an accepted Mean Organ Damage of 30%.

Prescribed doses to the Body were specified in this case with three **Quadratic Overdose Penalty** constraints: first with the 46 Gy reference dose and a RMS dose excess of 1 Gy to the whole volume 0,5 cm away from the target volumes (some space is needed in prder to have an achievable dose gradient), second with the reference dose 36 Gy and RMS limit of 1,5 Gy was applied to the area of the structure 1 cm away from the target volumes, and the third one with the reference dose of 30 Gy and a RMS dose excess of 1 Gy to the area 2,5 cm away from target volumes ("Shrink Margin" option).

As an example, the dose distribution for case B is presented on the Fig.4.7 (axial slice at the a height of a lymph nodes level). For this case several plans were obtained with Monaco™: with the constraints mentioned before and another one with **Multicriterial** optimization - option where the optimizer minimizes the dose for chosen OARs as far as possible. The third version was done with the employment of the Monte Carlo algorithm. Also from MasterPlan two plans were taken for comparison with two different optimizers. The results are presented

in the Table 4.2. It is necessary to mention that for all plans the PTV coverage was in a range of 96-99%.

	OMP Helax optimizer	OMP RaySearch optimizer	Monaco	Monaco Multicriterial	Monte Carlo optimized
D_{mean} to parotid	26,2Gy	23,9Gy	22,6Gy	23,1Gy	23,1Gy
D_{mean} to spinal cord	46,1Gy	39,8Gy	42,7Gy	39,4Gy	39,3Gy
D_{mean} to brain stem	46,7Gy	42,5Gy	45,4Gy	42,7Gy	41,3Gy
Number of segments/MU	87/507	97/558	96/884	86/1080	80/1102

Table 4.2: Plan evaluation results from 2 OMP optimizers and Monaco™.

4.1.3 Clinical case C (gynecological IMRT)

Radiation therapy for gynecological malignancies typically includes a combination of external beam irradiation (4-field technique or IMRT) and intracavitary brachytherapy. External beam therapy with doses in the range of 45-50 Gy is applied to the primary tumor/tumor bed and regional lymph nodes. Brachytherapy is used to boost dose to primary tumor safely to higher doses. The rationale for gynecological IMRT is reduced toxicity for normal tissues and reduced complications such as diarrhea, malabsorption, enteritis and proctitis for rectum and small bowel, fractures and necrosis for the femoral heads [50].

For this particular case the prescribed dose was 45 Gy in 25 fractions. Also a 7 beam arrangement was chosen with following gantry angles: $26° - 77° - 129° - 180° - 231° - 283° - 334°$. A 15 mm isotropic margin was applied to the CTV (1082,3 cm^3) to construct a PTV (2156,2 cm^3). The planning CT was performed with 4 mm slice thickness. Rectum, bladder and femoral heads were considered as OARs (see Fig. 4.8). Sigma and small bowel doses were reported but not included in prescription or optimization. The PTV for this case is partly overlapping with bladder, rectum, small bowel and includes almost the whole volume of the OAR sigma.

The prescription included 4 structures: PTV, rectum, bladder and external contour (Body). Three cost functions were assigned to the PTV:

- **Poisson Cell Kill Model** with an iso-constraint of 46.5 Gy (in order to prevent the loss of PTV coverage during the segmented optimization)
- **Quadratic Overdose Penalty** constraint with a reference dose of 47.5 Gy and 1.5 Gy RMS limit.
- **Maximum Dose Constraint** with an iso-constraint value of 51.5 Gy in order to prevent any dose higher than 115% of the prescribed dose.

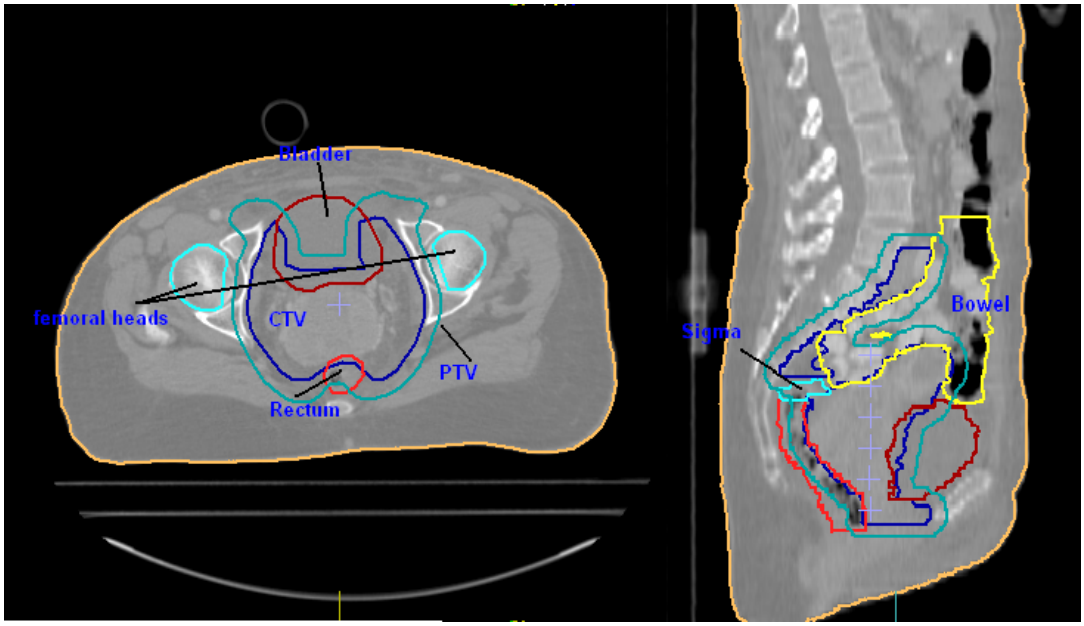

Figure 4.8: Target volumes and OARs delineation for gynecological case.

For bladder and rectum only the **Serial Complication Model** cost function was applied with different values of power law exponent. For the whole volume of the bladder the EUD was set to 42 Gy with a value of k =8. For the volume of bladder outside the PTV (expressed through 0.5 cm margin from the PTV in a cost function settings - "Shrink Margin" option) the EUD value was set to 30 Gy with a k-value of 12.

For the external contour the **Quadratic Overdose Penalty** constraint was used with the reference dose of 30 Gy and a RMS dose excess of 2 Gy, applied to the body area 1,5 cm away from target regions ("Shrink Margin" option). For the second stage of optimization a minimum segment size of 4 cm^2 was allowed with a minimum amount of 2 MU per segment and a segment suppression factor of 6.

The dose distribution for this case clearly represent sparing of the bladder and rectum, a minimization of the dose to femoral heads and bowel outside the PTV (see Fig. 4.9). The PTV coverage with 95% isodose (42,75 Gy) was 97%, absolute maximum dose was 51,26 Gy(113% from prescribed dose). Maximum OAR doses were 48,3 Gy for bladder and 45,9 Gy for rectum, mean dose to bowel - 28,5 Gy, mean doses for femoral heads - 34,4 Gy and 34,5 Gy for left and right femoral head, respectively.

Fig.4.10 shows the DVH comparison with plan optimization done in Oncentra MasterPlan 3.0 (RaySearch optimizer)(Nucletron, NL) and with Monaco™. As we can see there is no significant difference in PTV coverage (97,5% OMP vs. 97% Monaco™). The DVH for bowel and femoral heads also look very similar, but with Monaco™ we could achieve slightly better dose distributions for rectum and bladder (see Fig.4.11) These good results for Monaco™ are compromised when comparing MU. The OMP plan has only 450 MU for 115 segments while

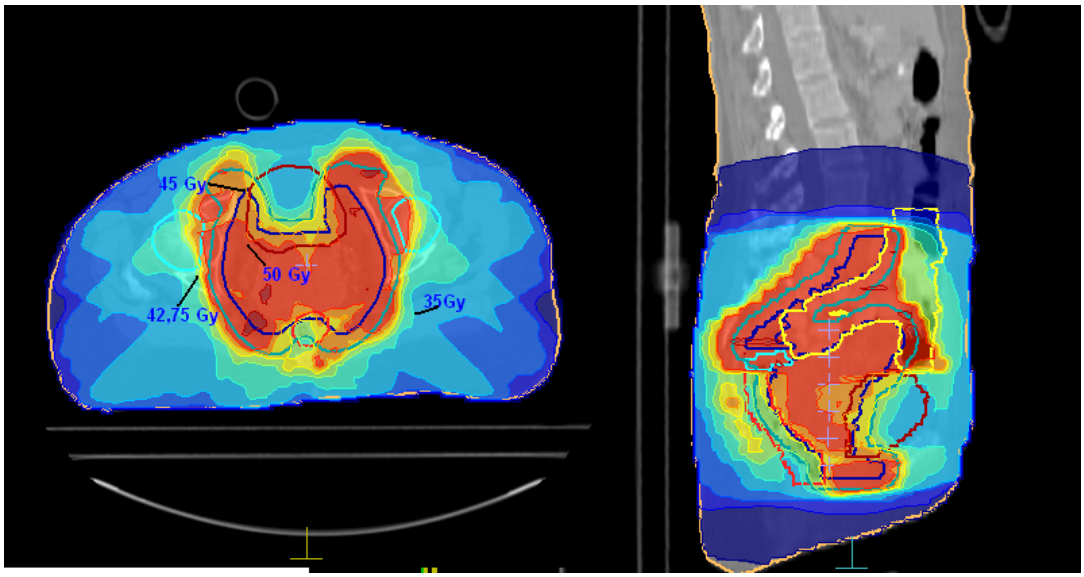

Figure 4.9: Dose distribution for gynecological case.

the biologically optimized plan has 92 segments with 789 MU.

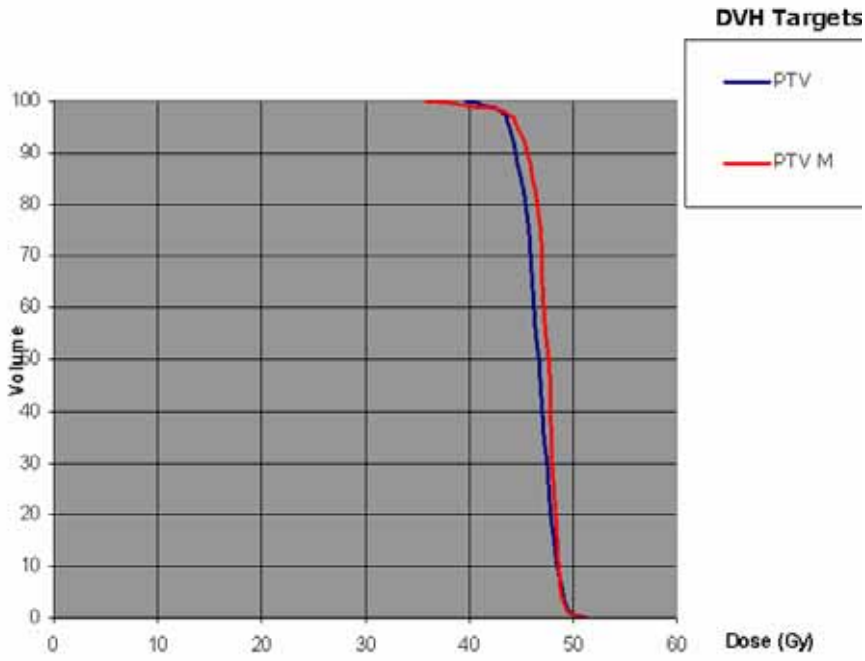

Figure 4.10: DVH comparison for target volume (blue line - Oncentra MasterPlan, red line - Monaco optimization results.

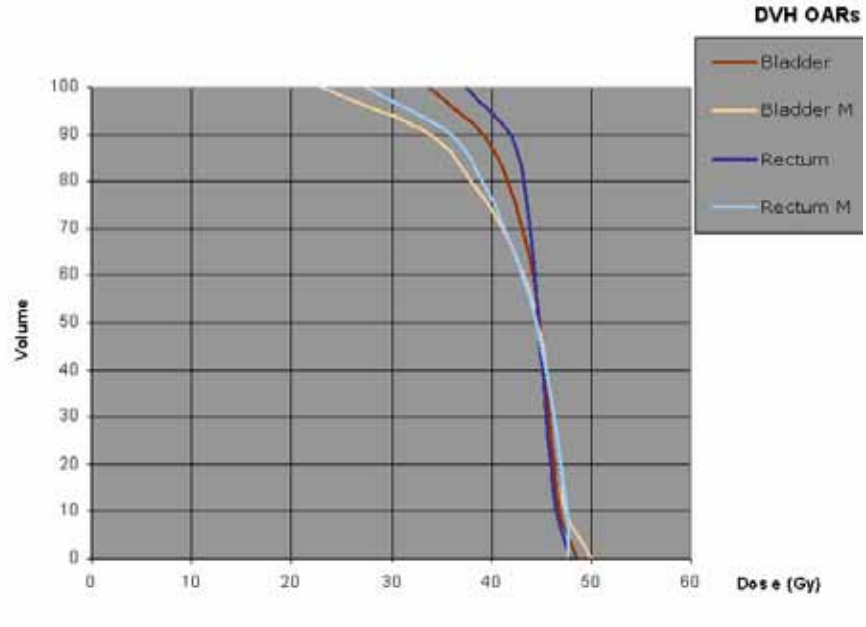

Figure 4.11: DVH for rectum (blue) and bladder (red), intense colors represent the results from MasterPlan, pale colors show Monaco DVHs.

Chapter 5

Summary and outlook

5.1 Summary

Intensity modulated radiotherapy (IMRT) is currently one of the most complex options in the treatment of cancer by ionizing radiation. It uses megavoltage photon beams of time-variable intensity patterns to further increase the conformity of three-dimensional conformal radiotherapy. This is especially helpful in case of concavely shaped tumour volumes with sensitive structures in their direct vicinity, since IMRT offers the possibility to "paint"' the high dose region following the target outline. Correspondingly, the exposure of organs at risk and normal tissue may be reduced without loosing tumour control. With the step-and-shoot multileaf collimation approach, intensity modulated beams are generated by superimposing several sub-fields or segments, individually shaped by a conventional multileaf collimator. Due to the vast number of degrees of freedom, in general computerized optimization algorithms are applied to find the optimal intensity distribution (inverse planning).

The aim of this thesis was to evaluate the treatment planning process and to perform measurements for the comissioning and pre-clinical verification of the TPS Monaco™.

Extensive literature research was performed in order to improve the understanding of the dose calculation algorithms and optimization solutions of the system. Monte Carlo dose calculation algorithms are considered as the most accurate dose calculation algorithms since they directly account for tissue heterogeneities and make no assumptions regarding radiation equilibrium. The wide application of these algorithms in clinical routine worldwide is a question of time.

Correct implementation of the Monte Carlo code in the TPS is a cruicial point for the reliability of the results. Hence, the quality of the beam data for the commissioning of the system and tests for the dosimetric accuracy of the system are very important an represent a major part of this thesis.

Within the scope of an optimizer study, an EUD-based formalism of the cost functions was

explored and evaluated as a convenient tool for expression of the clinical objectives. A so-called biological approach for the optimization, based on Critical Element and Critical Volume assumptions introduced additional flexibility in the planning process.

A patient-specific quality assurance (QA) procedure developed in Department of Radiotherapy Medical University of Vienna was used for the verification of Monaco™ plans. The verification was performed on the dedicated IMRT phantom. Within an in-house developed software package, the mathematical concept of γ-index distributions was used to quantitatively evaluate 2D dose distributions. The concept combines criteria for dose difference and distance to agreement (DTA), which are violated if the γ-index is larger than unity. Typical values are 3% and 3 mm for the dose difference and DTA criteria, respectively. An IMRT treatment plan is accepted if the following conditions are fulfilled: absolute deviation of number of MU $\pm$3%, less than 10% of measurement area with γ-values larger than unity, mean γ-value $\leq$0.6, and maximum g-value $\leq$2. Otherwise, the verification is repeated or the plan has to be re-optimized.

Finally, typical patient cases for different tumour entities (gynecological tumor and head-and-neck) were presented and compared with the results from the system Oncentra MasterPlan 3.0. The trial cases for Monaco™ optimization were taken from actual IMRT treatments and clearly illustrate possibilities of the TPS: concavely shaped high dose regions, sparing of organs at risk located close to the target or even (partially) surrounded by the tumour, sparing of normal tissue, tumour dose escalation, and application of simultaneous integrated boost techniques.

The created plans helped to develop a class of solutions with the optimally balanced outcome for timor coverage and sparing of the OARs. These results were introduces to the system as templates for IMRT planning.

5.2 Future research

The TPS Monaco™ proved to be a convenient and reliable tool for IMRT treatment planning. The use of this TPS for the planning problems of different complexity was successfully demonstrated. However, the small number of plans and especially phantom measurements for the dosimetric verification of the Monte Carlo algorithm open a wide field for the future research. The superiority of Monte Carlo for the dose calculation in region with tissue inhomogeneities should be evaluated on the detailed phantom study. At present time, we plan to perform a series of measurements with phantoms constructed from slabs of different densities and thorax verification phantom with cork mass and compare the dose calculation accuracy with more accurate fluence-based algoruthms.

Consequently, future investigations should deal with the influence of additional amount of MUs in treatment plans. The dosimetric aspects and determination of the optimization parameters helping to reduce MU is necessary before implementation the system in the routine.

The future studies of the influence of the different cost functions and their parameters on the

various patient's cases should lead to the establishment of the library of a "class solutions", making planning process more efficient.

Bibliography

[1] A. Ahnesjö. Collapsed cone convolution of radiant energy for photon dose calculation in heterogeneous media. *Med Phys*, 16:577–592, 1989.

[2] A. Ahnesjö, P. Andreo, and A. Brahme. Calculation and application of point spread functions for treatment planning with high energy photon beams. *Acta Oncol*, 26:49–56, 1987.

[3] M. Alber and F. Nüsslin. Intensity modulated photon beams subject to a minimal surface smoothing constraint. *Phys Med Biol*, 45:N49–N52, 2000.

[4] M. Alber and F. Nüsslin. Optimization of intensity modulated radiotherapy under constraints for static and dynamic mlc delivery. *Phys Med Biol*, 46:3229–3239, 2001.

[5] W. Bär, M. Alber, and F. Nüsslin. A variable fluence step clustering and segmentation algorithm for step and shoot IMRT. *Phys Med Biol*, 46:1997–2007, 2001.

[6] Bethesda, editor. *ICRU Report 50, Prescribing, Recording, and Reporting Photon Beam Therapy*. International Commission on Radiation Units and Measurements Washington DC, 1993.

[7] Bethesda, editor. *ICRU Report 62, Prescribing, Recording, and Reporting Photon Beam Therapy (supplement to ICRU report 50)*. International Commission on Radiation Units and Measurements Washington DC, 1999.

[8] T. Bortfeld, W. Schlegel, and B. Rhein. Decomposition of pencil beam kernels for fast dose calculations in three dimensional treatment planning. *Med Phys*, 20:311–318, 1993.

[9] T. Bortfeld, R. Schmidt-Ullrich, and D. E. Wazer, editors. *Image-Guided IMRT*. Springer-Verlag Berlin Heidelberg, 2006.

[10] A. Boyer and E. Mok. A photon dose distribution model employing convolution calculations. *Med Phys*, 12:169–177, 1985.

[11] A. Brahme. Dosimetric precision requirements in radiation therapy. *Acta Oncol.*, 23(5):379–391, 1984.

[12] A. Brahme, J. E. Roos, and I. Lax. Solution of an integral equation encountered in rotation therapy. *Phys Med Biol*, 27:1221–1229, 1982.

[13] M. Carol, W. H. Grant III, D. Pavord, P. Eddy, H. S. Targovnik, B. Butler, S. Woo, J. Figura, Y. Onufrey, R. Grossman, and R. Selkar. Initial clinical experience with the peacock intensity modulation of a 3-d conformal radiation therapy system. *Stereotact Funct Neurosurg*, 66:30–34, 1996.

[14] C. S. Chui, M. F. Chanf, E. Yorke, S. Spirou, and C. C. Ling. Delivery of intensity-modulated radiation therapy with a conventional multileaf collimator: comparison of dynamic and segmental methods. *Med. Phys.*, 28:2441–2449, 2001.

[15] A. M. Cormack and E. Quinto. On a problem in radiotherapy:questions on non-negativity. *Int J Imaging Syst Technol*, 1:120124, 1989.

[16] L. Cozzi, A. Fogliata nd F. Buffa, and S. Bieri. Dosimetric impact of computed tomography calibration on a commercial treatment planning system for external radiation therapy. *Radiother Oncol*, 48:355–338, 1998.

[17] J. Van Dyke, editor. *Modern technology of radiation oncology.* Medical Physics Publishing, Madison, Wisconsin, 1999.

[18] A. Eisbruch, R. K. Ten Haken, H. M. Kim, L. H. Marsh, and J. A. Ship. Dose, volume and function relationships in parotid salivary glands following conformal and intensity-modulated irradiation of head and neck cancer. *Int J Radiat Oncol Biol Phys*, 45:577–587, 1999.

[19] B. Emami and J. Lyman et al. Tolerance of normal tissue to therapeutic irradiation. *Int J Radiat Oncol Biol Phys*, 21:109122, 1991.

[20] G. De Meerleer et al. Direct segment aperture and weight optimization for intensity-modulated radiotherapy of prostate cancer. *Strahlenther Onkol*, 180(3):136–143, 2004.

[21] G. Schoknecht et al. Description of radiation fields by separation of primary and scatter radiation. *Strahlentherapie*, 132:516–528, 1967.

[22] L. Xing et al. Monitor unit calculation for an intensity modulated photon field by a simple scatter-summation algorithm. *Phys Med Biol*, 45(3):N1–N7, 2000.

[23] Y. Yang et al. Independent dosimetric calculation with inclusion of head scatter and MLC transmission for IMRT. *Med Phys*, 30(11):2937–2947, 2003.

[24] M. Fippel. Fast Monte Carlo dose calculation for photon beams based on the VMC electron algorithm. *Med Phys*, 26:1466–1475, 1999.

[25] M. Fippel. Inverse treatment planning for radiation therapy based on fast Monte Carlo dose calculation. In *Monte Carlo 2000 Conference, Lisbon. Springer, Berlin Heidelberg New York*, 2000.

[26] M. Fippel. Efficient particle transport simulation through beam modulating devices for monte carlo treatment planning. *Med. Phys.*, 31:1235–1242, 2004.

[27] M. Fippel, F. Haryanto, O. Dohm, F. Nüsslin, and S. Kriesen. A virtual photon energy fluence model for monte carlo dose calculation. *Med. Phys.*, 30:301–311, 2003.

[28] D. Georg and B. Kroupa. Pre-clinical evaluation of an inverse planning module for segmental MLC based IMRT delivery. *Phys. Med. Biol.*, 47:303–314, 2002.

[29] D. Georg, M. Stock, B. Kroupa, J. Olofsson, T. Nyholm, A. Ahnesjö, and M. Karlsson. Patient-specific IMRT verification using independent fluence-based dose calculation software: experimental benchmarking and initial clinical experience. *Phys. Med. Biol.*, 52:4981–4992, 2007.

[30] D. Georg, T.Nyholm, and J. Oloffson et al. Clinical evaluation of the monitor unit software and the application of action levels. *Radiother. Oncol.*, 85(2):306–315, 2007.

[31] V. Gregoire, A. Eisbruch, M. Hamoir, and P. Levendag. Proposal for the delineation of the nodal ctv in the node-positive and the post-operative neck. *Radiother. Oncol.*, 79(1):15–20, 2006.

[32] U. Jelen and M. Alber. A finite size pencil beam algorithm for IMRT dose optimization: density corrections. *Phys Med Biol*, 52:617–633, 2007.

[33] U. Jelen, M. Söhn, and M. Alber. A finite size pencil beam for IMRT dose optimization. *Phys Med Biol*, 50:1747–1766, 2005.

[34] H. Jiang, J. Seco, and H. Paganetti. Effects of hounsfield number conversion on ct based proton monte carlo dose calculations. *Med. Phys.*, 34(4):1439–1449, 2007.

[35] I. Kawrakow and M. Fippel. VMC++, a fast MC algorithm for radiation treatment planning. In *XIII International Conference on the Use of Computers in Radiation Therapy. Springer, Berlin Heidelberg New York*, 2000.

[36] E. Klein, Z. Li, and J. Jin. Reduction of IMRT patient quality assurance by means of independent dose calculations (abstract). *Med. Phys.*, 30:1496, 2003.

[37] B. Kroupa. *Diss. Clinical implementation of the intensity modulated radiotherapy based on segmental multileaf collimator.* Vienna University of Technology, 2005.

[38] G. J. Kutcher and C. Burman. Calculation of complication probability factors for non-uniform normal tissue irradiation: the effective volume method. *Int J Radiat Oncol Biol Phys*, 16:16231630, 1989.

[39] S. H. Levitt, J. A. Purdy, C. A. Perez, and S. Vijayakumar, editors. *Technical Basis of Radiation Therapy,4th edition.* Springer-Verlag Berlin Heidelberg New-York, 2006.

[40] Y. Li, J. M. Taylor, R. K. Ten Haken, and A. Eisbruch. The impact of dose on parotid salivary recovery in head and neck cancer patients treated with radiation therapy. *Int J Radiat Oncol Biol Phys*, 67:660–669, 2007.

[41] T. LoSasso, C. S. Chui, and C. C. Ling. Physical and dosimetric aspects of a multileaf collimation system used in the dynamic mode for implementing intensity modulated radiotherapy. *Med. Phys.*, 25:1919–1927, 1998.

[42] D. A. Low, W. B. Harms, S. Mutic, and J. A. Purdy. A technique for the quantitative evaluation of dose distributions. *Med. Phys.*, 25:656–661, 1998.

[43] J. T. Lyman. Complication probability as assessed from dose-volume histograms. *Radiat Res Suppl*, 8:S13S19, 1985.

[44] T. R. Mackie, J. Balog, K. Ruchala, D. Shepard, S. Aldridge, E. Fitchard, P.J. Reckwerdt, G. Olivera, T. R. McNutt, and M. Metha. Tomotherapy. *Semin Radiat Oncol*, 9:108–117, 1999.

[45] T. R. Mackie, T. Holmes, S. Swerdloff, P. Reckwerdt, J. O. Deasy, J. Yang, B. Paliwal, and T. Kinsella. Tomotherapy: a new concept for the delivery of conformal radiotherapy using dynamic collimation. *Med. Phys.*, 20:1709–1719, 1993.

[46] T. R. Mackie and J. R. Palta, editors. *Teletherapy: present and future*. Advanced Medical Publishing, Madison,WI, 1996.

[47] T. R. Mackie, J. W. Scrimger, and J. J. Battista. A convolution method of calculating dose for 15-MV X-rays. *Med Phys*, 12:188–196, 1985.

[48] R. Mohan, C. Chui, and L. Lidofsky. Differential pencil beam dose computation model for photons. *Med Phys*, 13:64–73, 1986.

[49] A. J. Mundt. *Intensity Modulated Radiation Therapy: A Clinical Perspective*. BC Decker Inc, 2005.

[50] A. J. Mundt, J. C. Roeske, and A. E. Lujan. Intensity-modulated radiation therapy in gynecologic malignancies. *Med Dosim*, 27:131–136, 2002.

[51] A. Niemierko. Reporting and analyzing dose distributions: a concept of equivalent uniform dose. *Med. Phys.*, 24:103–110, 1997.

[52] A. Niroomand-Rad, C. Blackwell, B. Coursey, K. Gall, and J. Galvin et al. Radiochromic film dosimetry: recommendation of AAPM radiation therapy task group 55. *Med. Phys.*, 25:2093–2115, 1998.

[53] L. Paelink, N. Reynaert, H. Thierens, C. DeWagter, and W. De Neve. The value of radiochromic film dosimetry around air cavities: experimental results and monte carlo simulations. *Phys Med Biol*, 48:1895–1905, 2003.

[54] E. B. Podgorsak, editor. *Radiation Oncology Physics: a handbook for teachers and students*. IAEA Vienna Austria, 2005.

[55] W. H. Press, B. P. Flannery, S. A. Teukolsky, and W. T. Vetterling. *Numerical recipes in C: the art of scientific computing*. Cambridge University Press, Cambridge, 1992.

[56] D. W. O. Rogers, B. A. Faddegon, G. X. Ding, C. M. Ma, J. Wei, and T. R. Mackie. BEAM: a monte carlo code to simulate radiotherapy treatment units. *Med. Phys.*, 22:503–524, 1995.

[57] W. Schlegel, T. Bortfeld, and A.-L. Grosu, editors. *New Technologies in Radiation Oncology*. Springer Berlin New York, 2006.

[58] U. Schneider, E. Pedroni, and A. Lomax. The calibration of ct hounsfield units for radiotherapy treatment planning. *Phys Med Biol*, 41:111–124, 1996.

[59] C. Scholz, S. Nill, and U. Oelfke. Comparison of IMRT optimization based on a pencil beam and a superposition algorithm. *Med Phys*, 30:1909–1913, 2003.

[60] J. Sempau and A. F. Bielajew. Towards the elimination of monte carlo statistical fluctuation from dose volume histograms for radiotherapy treatment planning. *Phys Med Biol*, 45:131–157, 2000.

[61] IAEA TEC-DOC Series. *Specification and Acceptance Testing of Radiotherapy Treatment Planning Systems*. International Atomic Energy Agency, Vienna, Austria, 2007.

[62] J. V. Siebers and at al. Acceleration of dose calculations for intensity-modulated radiotherapy. *Med Phys*, 28:903–910, 2001.

[63] J. Stein, R. Mohan, X.H. Wang, T.Bortfeld, and Q. Wu et al. Number and orientations of beams in intensity-modulated radiation treatments. *Med. Phys.*, 24:149–160, 1997.

[64] M. Stock. *Diploma thesis. Implementierung eines Güteparameters zur Beurteilung von Bestrahlungplänen in der IMRT*. Vienna University of Technology, 2003.

[65] M. Stock, B. Kroupa, and D. Georg. Interpretation and evaluation of the γ index and the γ index angle for the verification of IMRT hybrid plans. *Phys. Med. Biol.*, 50(3):399–411, 2005.

[66] E. Sturtenwagen. *Diploma thesis. Verification of stereotactic radiotherapy for uveal melanoma using radiochromic film dosimetry*. University of Ghent, 2006.

[67] S. J. Thomas. Relative electron density calibration of ct scanners for radiotherapy treatment planning. *Br J Radiol*, 72:781–786, 1999.

[68] A. Van Esch, T. Depuydt, and D. P. Huyskens. The use of an aSi-based EPID for routine absolute dosimetric pre-treatment verification of dynamic IMRT fields. *Radiother. Oncol.*, 71(2):223–234, 2004.

[69] L. Wang, J. Li, and K. Paskalev at al. Commissioning and quality assurance of a commercial stereotactic treatment planning system for extracranial IMRT. *J App Clin Med Phys*, 7(1):14–28, 2006.

[70] S. Webb. *The physics of conformal radiotherapy: advances in technology.* IOP Publishing Bristol, 1997.

[71] S. Webb. *Intensity modulated radiation therapy.* IOP Publishing Bristol, 2000.

[72] S. Webb. *Contemporary IMRT Developing Physics and Clinical implementation.* IOP Publishing Bristol, 2004.

[73] H. R. Withers and J. M. Taylor et al. Treatment volume and tissue tolerance. *Int J Radiat Oncol Biol Phys*, 14:751759, 1988.

[74] S. Y. Woo, M. Sanders, W. Grant, and E. B. Butler. Does the "peacock" have anything to do with radiotherapy? *Int J Radiat Oncol Biol Phys*, 29:213–214, 1994.

[75] Q. Wu and at al. A fast dose calculation method based on table lookup for IMRT optimization. *Phys Med Biol*, 48:N159–N166, 2003.

[76] Q. Wu, M. Manning, R. Schmidt-Ullrich, and R. Mohan. The potential of sparing of parotids and escalation of biologically effective dose with IMRT of head and neck cancer: a treatment design study. *Int J Radiat Oncol Biol Phys*, 46:195–205, 2000.

[77] Q. Wu and R. Mohan. Algorithms and functionality of an intensity modulated radiotherapy optimization system. *Med Phys*, 27:701–711, 2000.

[78] Q. Wu, R. Mohan, A. Niemierko, and R. Schmidt-Ullrich. Optimization of intensity-modulated radiotherapy plans based on the equivalent uniform dose. *Int J Radiat Oncol Biol Phys*, 52:224235, 2002.

[79] C. X. Yu. Intensity-modulated arc therapy with dynamic multileaf collimation: an alternative to tomotherapy. *Phys Med Biol*, 40:1435–1449, 1995.

[80] C. X. Yu, X. A. Li, L. Ma, D. Chen, S. Nagvi, D. Shepard, M. Sarfaraz, T. W. Holmes, M. Suntharalingam, and C. M. Mansfield. Clinical implementation of intensity-modulated arc therapy. *Int J Rad Oncol Biol Phys*, 53(2):453–463, 2002.

[81] X. Zhang, H. Liu, , L. Dong, Q. Wu, and R. Mohan. Speed and convergence properties of gradient algorithms for optimization of IMRT. *Med. Phys.*, 31:1141–1152, 2004.